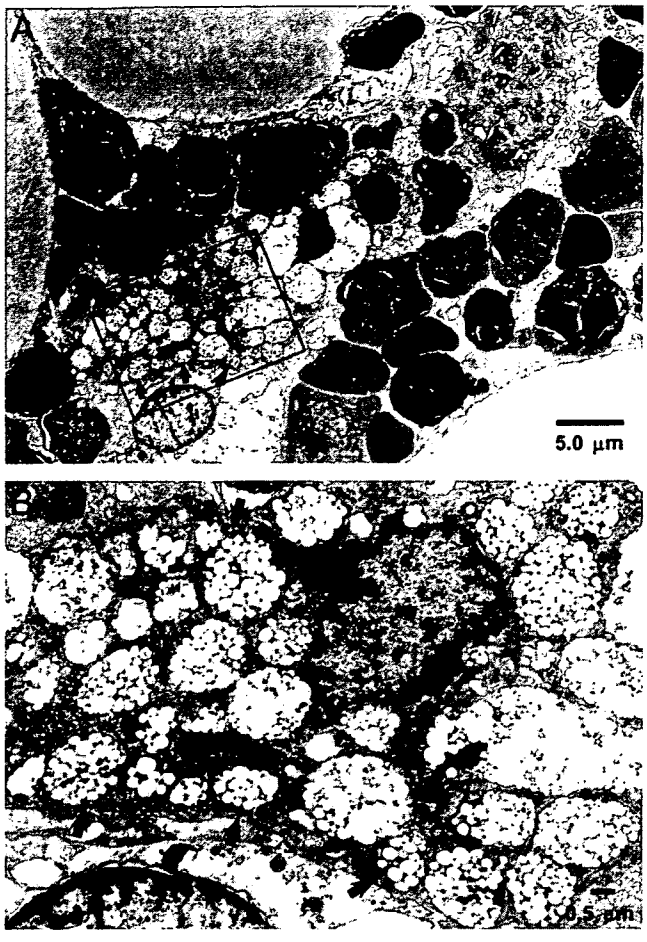


Fig. 6. Transmission electron micrographs of femoral bone marrow tissue section, taken from rabbit at 6 h after i.v. injection of PEG(0.6)-[SA-Ve] (lipids: 15 mg/kg b.w.). (A) Low magnified micrograph representing the bone marrow tissue including macrophage and various bone marrow cells. (B) High magnified micrograph of framed region in panel (A). A massive number of vesicles with original diameter (average 270 nm) are trapped in several endosomes or lysosomes of macrophage. Some are indicated by arrows, which shows same position in (A) and (B).

uptake of PEG(0.6)-[SA-Ve] by bone marrow was responded by the endocytosis of BMM$\phi$. One potent trigger to accelerate the cellular endocytosis for vesicles is an interaction with the receptors on the surface of cells, that are known as a receptor-mediated endocytosis which is investigated as a potent pathway for drug targeting to specific cell including macrophage [2,10,11]. Scavenger receptors are membrane glycoproteins that are present mainly on cells of the macrophage lineage [35,36]. Various polyanionic compounds such as dextran sulfate, polyinosinic acid, and acetylated low density lipoproteins have been reported as ligands for this receptor [37,38]. These compounds are taken at high levels by macrophages via a scavenger receptor-mediated mechanism. On the other hand, many polyanions such as chondroitin sulfate, poly(D-glutamic) acid, and polycytidylic acid are not ligands for scavenger receptors [37,38]. Previous investigations indicated that the scavenger receptors on macrophages contribute to the recognition of polyanionic structures, resulting in selective uptake. Enhanced uptake of succinylated proteins has been investigated in cultured brain microvessel endothelial cells. Endothelial cells also express the scavenger receptor on their surface. Large succinylated proteins such as catalase (Mw 227 kDa) and bovine serum albumin (Mw 70 kDa) were taken up by the cells via a scavenger receptor-mediated mechanism, whereas significant uptake was not observed for native proteins and small succinylated proteins such as SOD (Mw 34 kDa) and soybean trypsin inhibitor (Mw 21 kDa) [39]. This indicates that succinylation of large molecules is involved in the uptake via a scavenger receptor-mediated mechanism. Recently, Szabó et al. reported the uptake of branched polypeptides by bone marrow culture-derived murine macrophages. They indicated that the succinylation of branched polypeptides significantly enhanced the uptake by macrophages, and the uptake was inhibited by blocking of the class-A scavenger receptors [40]. Because the terminal hydrophilic head group of SA is corresponding to the succinylated structure, we speculate that the interaction between PEG-[SA-Ve] and the scavenger receptors on BMM$\phi$ might participate in the selective uptake. However, further mechanistic investigation on uptake of PEG-[SA-Ve] by BMM$\phi$, splenic macrophages, and hepatic Kupffer cells is necessary to clarify the mechanism of organ selective macrophage uptake.

Previous pharmacokinetic studies have been performed using vesicles containing SA that have the same lipid composition as in the present study with PEG(0.3)-[SA-Ve], but a significantly higher dose was employed (lipids: 680 mg/kg b.w.) [17]. In these studies, the bone marrow-selective distribution was not observed, so it appears that the bone marrow selectivity is limited by the injection dosage in certain applications. As the vesicle dosage increases, the MPS in the bone marrow becomes saturated; as a result, liver and spleen uptake is increased. In our previous organ distribution study in rabbits, >50%ID of the vesicles were still in circulation at 48 h after infusion of a massive dose of vesicles, while the bone marrow had $7.36 \pm 0.34\%$ of 680 mg/kg b.w. at the same time point [17]. This value is equivalent to 50.0 mg/kg b.w., and it can be used to estimate the maximum uptake capacity of MPS for vesicles. When vesicle dosage increases above 50.0 mg/kg b.w., the bone marrow is the first organ to become saturated, and the accumulation of vesicles then increases in the liver and spleen. Such sequential saturation of the MPS eliminates organ selectivity. Therefore, the bone marrow targeting of SA-Ve becomes striking when the dose of vesicles is below the saturation dosage for bone marrow, as observed in the present study (15 mg/kg b.w.). The ability of vesicular nanoparticles to encapsulate a wide variety of agents provides significant opportunities for bone marrow delivery applications. In the present study, we have demonstrated the delivery of scintigraphic and fluorescence imaging agents to bone marrow by using the

SA-Ve vesicles. This method has advantages in delivering the therapeutic agents to treat bone marrow disorders.

## 5. Conclusion

This is the first report to show the organ distribution of PEG-[SA-Ve] at small dose injection. Organ distributions of several vesicular formulations were quantitatively compared to determine the component to induce the significant distribution into bone marrow. Our data have indicated that surface modification of phospholipid vesicles with two compounds, SA and PEG-DSPE, cooperatively induces the significant bone marrow targeting properties to vesicles. In this system, BMM$\phi$ participated in the uptake of PEG-[SA-Ve], and the efficient delivery of the vesicles as encapsulating agents into the bone marrow was achieved within 6 h after injection. These results indicated that the PEG-[SA-Ve] is a potent carrier for drug delivery into BMM$\phi$ *in vivo* and may be useful for delivering a wide range of therapeutic agents to bone marrow.

## Acknowledgments

This work was partly supported by project of a Health and Labor Sciences Research Grant (Research on Pharmaceutical and Medical Safety, Artificial Blood Project) of the Ministry of Health, Labor and Welfare, Japan, and the Ministry of Education, Culture, Sports, Science and Technology, Grant-in-Aid for Scientific Research (B), 17300162, 2005. The authors gratefully acknowledge Dr. H. Sakai (Waseda University) for discussions on this research, Dr. Linda M. McManus (UTHSCSA) for assistance with electron microscopic images and Mr. R. Klipper (UTHSCSA) for technical support.

## Appendix A. Supplementary materials

The online version of this article contains additional supplementary data. Please visit doi:10.1016/j.biomaterials.2007.01.041.

## References

[1] Farokhzad OD, Jon S, Khademhosseini A, Tran TN, Lavan DA, Langer R. Nanoparticle–aptamer bioconjugates: a new approach for targeting prostate cancer cells. Cancer Res 2004;64:7668–72.

[2] Torchilin VP. Recent advances with liposomes as pharmaceutical carriers. Nat Rev Drug Discov 2005;4:145–60.

[3] Gregoriadis G, Wills EJ, Swain CP, Tavill AS. Drug-carrier potential of liposomes in cancer chemotherapy. Lancet 1974;1:1313–6.

[4] Felgner PL, Gadek TR, Holm M, Roman R, Chan HW, Wenz M, et al. Lipofection: a highly efficient, lipid-mediated DNA-transfection procedure. Proc Natl Acad Sci USA 1987;84:7413–7.

[5] Moghimi SM, Hunter AC, Murray JC. Long-circulating and target-specificity nanoparticles: theory to practice. Pharmacol Rev 2001;53:283–318.

[6] Sakai H, Horinouchi H, Tomiyama K, Ikeda E, Takeoka S, Kobayashi K, et al. Hemoglobin-vesicles as oxygen carriers: influence on phagocytic activity and histopathological changes in reticuloendothelial system. Am J Pathol 2001;159:1079–88.

[7] Fadok VA, Bratton DL, Rose DM, Pearson A, Ezekewitz RA, Henson PM. A receptor for phosphatidylserine-specific clearance of apoptotic cells. Nature 2000;405:85–90.

[8] Klibanov AL, Maruyama K, Torchilin VP, Huang L. Amphipathic polyethyleneglycols effectively prolong the circulation time of liposomes. FEBS Lett 1990;268:235–7.

[9] Gabizon A, Shmeeda H, Barenholz B. Pharmacokinetics of pegylated liposomal Doxorubicin: review of animal and human studies. Clin Pharmacokinet 2003;42:419–36.

[10] Turk MJ, Water DJ, Low PS. Folate-conjugated liposomes preferentially target macrophages associated with ovarian carcinoma macrophage. Cancer Lett 2004;213:165–72.

[11] Chellat F, Merhi Y, Moreau A, Yahia L'H. Therapeutic potential of nanoparticulate systems for macrophage targeting. Biomaterials 2005;26:7260–75.

[12] Mantovani A, Sozzani S, Locati M, Allavena P, Sica A. Macrophage polarization: tumor-associated macrophages as a paradigm for polarized M2 mononuclear phagocytes. Trends Immunol 2002;23:549–55.

[13] Allen TM, Austin GA, Chonn A, Lin L, Lee KC. Uptake of liposomes by cultured mouse bone marrow macrophages: influence of liposome composition and size. Biochim Biophys Acta 1991;1061:56–64.

[14] Phillips WT, Klipper RW, Awasthi VD, Rudolph AS, Cliff R, Kwasiborski V, et al. Polyethylene glycol-modified liposome-encapsulated hemoglobin: a long circulating red cell substitute. J Pharmacol Exp Ther 1999;288:665–70.

[15] Dams ET, Oyen WJ, Boerman OC, Storm G, Laverman P, Kok PJ, et al. $^{99m}$Tc-PEG liposomes for the scintigraphic detection of infection and inflammation: clinical evaluation. J Nucl Med 2000;41:622–30.

[16] Giuliani AL, Wiener E, Lee MJ, Brown IN, Berti G, Wickramasinghe SN. Changes in murine bone marrow macrophages and erythroid burst-forming cells following the intravenous injection of liposome-encapsulated dichloromethylene diphosphonate ($Cl_2$MDP). Eur J Haematol 2001;66:221–9.

[17] Sou K, Klipper R, Goins B, Tsuchida E, Phillips WT. Circulation kinetics and organ distribution of Hb-vesicles developed as a red blood cell substitute. J Pharmacol Exp Ther 2005;312:702–9.

[18] Sadahira Y, Mori M. Role of the macrophage in erythropoiesis. Pathol Int 1999;49:841–8.

[19] Yoshida H, Kawane K, Koike M, Mori Y, Uchiyama Y, Nagata S. Phosphatidylserine-dependent engulfment by macrophages of nuclei from erythroid precursor cells. Nature 2005;437:754–8.

[20] Sou K, Naito Y, Endo T, Takeoka S, Tsuchida E. Effective encapsulation of proteins into size-controlled phospholipid vesicles using freeze–thawing and extrusion. Biotechnol Prog 2003;19:1547–52.

[21] Sou K, Endo T, Takeoka S, Tsuchida E. Poly(ethylene glycol)-modification of the phospholipid vesicles by using the spontaneous incorporation of poly(ethylene glycol)-lipid into the vesicles. Bioconjug Chem 2000;11:372–9.

[22] Sakai H, Hisamoto S, Fukutomi I, Sou K, Takeoka S, Tsuchida E. Detection of lipopolysaccharide in hemoglobin-vesicles by Limulus amebocyte lysate test with kinetic-turbidimetric gel clotting analysis and pretreatment of surfactant. J Pharm Sci 2004;93:310–21.

[23] Rudolph AS, Klipper R, Goins B, Phillips WT. *In vivo* biodistribution of a radiolabeled blood substitute: $^{99m}$Tc-labeled liposome-encapsulated hemoglobin in an anesthetized rabbit. Proc Natl Acad Sci USA 1991;88:10976–80.

[24] Phillips WT, Rudolph AS, Goins B, Timmons JH, Klipper R, Blumhardt R. A simple method for producing a technetium-99m-labeled liposome which is stable *in vivo*. Nucl Med Biol 1992;19:539–47.

[25] Awasthi V, Goins B, Klipper R, Loredo R, Korvick D, Phillips WT. Dual radiolabeled liposomes: biodistribution studies and localization of focal sites of infection in rats. Nucl Med Biol 1998;25:155–60.
[26] Kozma C, Macklin W, Cummins LM, Mauer R. Anatomy, physiology, and biochemistry of the rabbit. In: Weisbroth SH, Flatt RE, Kraus AL, editors. The biology of the laboratory rabbit. New York: Academic Press; 1974. p. 50–69.
[27] Kaplan HM, Timmons EH. The rabbit: a model for the principles of mammalian physiology and surgery. New York: Academic Press; 1979.
[28] Deitz AA. Distribution of bone marrow, bone and bone ash in rabbits. Proc Soc Exp Med 1944;57:60–2.
[29] Lefevre C, Kang HC, Haugland RP, Malekzadeh N, Arttamangkul S, Haugland RP. Texas Red-X and rhodamine Red-X, new derivatives of sulforhodamine 101 and lissamine rhodamine B with improved labeling and fluorescence properties. Bioconjug Chem 1996;7:482–9.
[30] Torchilin VP, Papisov MI. Why do polyethylene glycol-coated liposomes circulate so long? J Liposome Res 1994;4:725–39.
[31] Du H, Chandaroy P, Hui SW. Grafted poly-(ethylene glycol) on lipid surface inhibits protein adsorption and cell adhesion. Biochim Biophys Acta 1997;1326:236–48.
[32] Edholm O, Nagle JF. Areas of molecules in membranes consisting mixtures. Biophys J 2005;89:1827–32.
[33] Awasthi VD, Garcia D, Klipper R, Goins BA, Phillips WT. Neutral and anionic liposome-encapsulated hemoglobin: effect of postinserted poly(ethylene glycol)-distearoylphosphatidylethanolamine on distribution and circulation kinetics. J Pharmacol Exp Ther 2004; 309:241–8.
[34] Awasthi VD, Garcia D, Goins BA, Phillips WT. Circulation and biodistribution profiles of long-circulating PEG-liposomes of various sizes in rabbits. Int J Pharm 2003;253:121–32.
[35] Doi T, Higashino K, Kurihara Y, Wada Y, Miyazaki T, Nakamura H, et al. Charged collagen structure mediates the recognition of negatively charged macromolecules by macrophage scavenger receptors. J Biol Chem 1993;268:2126–33.
[36] Taylor PR, Martinez-Pomares L, Stacey M, Lin HH, Brown GD, Gordon S. Macrophage receptors and immune recognition. Annu Rev Immunol 2005;23:901–44.
[37] Brown MS, Goldstein JL. Lipoprotein metabolism in the macrophage: implications for cholesterol deposition in atherosclerosis. Annu Rev Biochem 1983;52:223–61.
[38] Krieger M, Acton S, Ashkenas J, Pearson A, Penman M, Resnick D. Molecular flypaper, host defense, and atherosclerosis. Structure, binding properties, and functions of macrophage scavenger receptors. J Biol Chem 1993;268:4569–72.
[39] Tokuda H, Masuda S, Takakura Y, Sezaki H, Hashida M. Specific uptake of succinylated proteins via a scavenger receptor-mediated mechanism in cultured brain microvessel endothelial cells. Biochem Biophys Res Commun 1993;196:18–24.
[40] Szabó R, Peiser L, Plüddemann A, Bösze S, Heinsbroek S, Gordon S, et al. Uptake of branched polypeptides with poly[L-lys] backbone by bone-marrow culture-derived murine macrophages: the role of the class a scavenger receptor. Bioconjug Chem 2005;16:1442–50.

# Rheological Properties of Hemoglobin Vesicles (Artificial Oxygen Carriers) Suspended in a Series of Plasma-Substitute Solutions

Hiromi Sakai,[†] Atsushi Sato,[‡] Shinji Takeoka,[‡] and Eishun Tsuchida*,[†]

*Advanced Research Institute for Science and Engineering and Graduate School of Science and Engineering, Waseda University, Tokyo 169-8555, Japan*

*Received February 15, 2007. In Final Form: April 3, 2007*

Hemoglobin vesicles (HbV) or liposome-encapsulated Hbs are artificial oxygen carriers that have been developed for use as transfusion alternatives. The extremely high concentration of the HbV suspension (solutes, ca. 16 g/dL; volume fraction, ca. 40 vol %) gives it an oxygen-carrying capacity that is comparable to that of blood. The HbV suspension does not possess a colloid osmotic pressure. Therefore, HbV must be suspended in or co-injected with an aqueous solution of a plasma substitute (water-soluble polymer), which might interact with HbV. This article describes our study of the rheological properties of HbV suspended in a series of plasma substitute solutions of various molecular weights: recombinant human serum albumin (rHSA), dextran (DEX), modified fluid gelatin (MFG), and hydroxylethyl starch (HES). The HbV suspended in rHSA was nearly Newtonian. Other polymers—HES, DEX, and MFG—induced HbV flocculation, possibly by depletion interaction, and rendered the suspensions as non-Newtonian with a shear-thinning profile ($10^{-4}$−$10^{3}$ $s^{-1}$). These HbV suspensions showed a high storage modulus ($G'$) because of the presence of flocculated HbV. However, HbV suspended in rHSA exhibited a very low $G'$. The viscosities of HbV suspended in DEX, MFG, and high-molecular-weight HES solutions responded quickly to rapid step changes in shear rates of 0.1−100 $s^{-1}$ and a return to 0.1 $s^{-1}$, indicating that flocculation is both rapid and reversible. Microscopically, the flow pattern of the flocculated HbV that perfused through microchannels (4.5 $\mu$m deep, 7 $\mu$m wide, 20 cm$H_2O$ applied pressure) showed no plugging. Furthermore, the time required for passage was simply proportional to the viscosity. Collectively, the HbV suspension viscosity was influenced by the presence of plasma substitutes. The HbV suspension provides a unique opportunity to manipulate rheological properties for various clinical applications in addition to its use as a transfusion alternative.

## Introduction

Phospholipid vesicles or liposomes encapsulating or embedding functional drugs or biological materials have been investigated aggressively for use in drug-delivery systems; some were subsequently approved for antifungal or anticancer therapy.[1] Hemoglobin vesicles (HbV) are artificial oxygen carriers that encapsulate a concentrated Hb solution in phospholipid vesicles (280 nm particle diameter).[2−6] Their oxygen-carrying capacity and safety as a transfusion alternative have been evaluated energetically in animal tests aimed at clinical applications. In contrast to conventional liposomal products, the concentration of the HbV suspension must be extremely high (Hb, 10 g/dL; lipids, 5−6 g/dL); one injection as a transfusion alternative causes the substitution of a large volume of blood: about 40% of the circulating blood volume.[7] Accordingly, it is important to evaluate its safety not only in terms of the biocompatibility of the HbV particles themselves but also in terms of the rheological property of the HbV suspension, the infusion fluid, compared to the blood hemorheology.[8−10]

Albumin, dissolved in a blood plasma at ca. 5 g/dL, provides sufficient colloid osmotic pressure (COP, ca. 20 Torr) to play an important role in equilibrating COP between blood and interstitial fluid, thereby maintaining the overall blood volume. This COP is one requisite for a transfusion alternative to sustain blood circulation for transporting oxygen and metabolites. One HbV contains about 30 000 Hb molecules. Therefore, an HbV suspension shows no COP in an aqueous solution. Accordingly, HbV must be suspended in or co-injected with a plasma substitute solution. This requirement is identical to that for emulsified perfluorocarbon, which does not possess COP;[11,12] it contrasts with characteristics of other Hb-based oxygen carriers (HBOCs), intramolecular cross-linked Hbs, polymerized Hbs, and polymer-conjugated Hbs, which all possess very high COP as protein solutions.[13−15]

Animal tests of HbV suspended in plasma-derived human serum albumin (HSA) or recombinant HSA (rHSA) showed an oxygen-transporting capacity that is comparable to that of

* To whom correspondence should be addressed. E-mail: eishun@waseda.jp. Tel: +81-3-5286-3120. Fax: +81-3-3205-4740.

[†] Advanced Research Institute for Science and Engineering.

[‡] Graduate School of Science and Engineering.

(1) Torchilin, V. P. *Nat. Rev. Drug Discovery* **2005**, *4*, 145−160.

(2) Izumi, Y.; Sakai, H.; Hamada, K.; Takeoka, S.; Yamahata, T.; Kato, R.; Nishide, H.; Tsuchida, E.; Kobayashi, K. *Crit. Care Med.* **1996**, *24*, 1869−1873.

(3) Sakai, H.; Takeoka, S.; Park, S. I.; Kose, T.; Nishide, H.; Izumi, Y.; Yoshizu, A.; Kobayashi, K.; Tsuchida, E. *Bioconjugate Chem.* **1997**, *8*, 23−30.

(4) Chang, T. M. *Artif. Organs* **2004**, *28*, 789−794.

(5) Djordjevich, L.; Miller, I. F. *Exp. Hematol.* **1980**, *8*, 584−592.

(6) Phillips, W. T.; Klipper, R. W.; Awasthi, V. D.; Rudolph, A. S.; Cliff, R.; Kwasiborski, V.; Goins, B. A. *J. Pharmacol. Exp. Ther.* **1999**, *288*, 665−670.

(7) Sakai, H.; Horinouchi, H.; Yamamoto, M.; Ikeda, E.; Takeoka, S.; Takaori, M.; Tsuchida, E.; Kobayashi, K. *Transfusion* **2006**, *46*, 339−347.

(8) Makino, C.; Kimura, N.; Hasegawa, E.; Tsuchdia. E. *Nippon Kagaku Kaishi* **1991**, *8*, 1102−1105.

(9) Sakai, H.; Hamada, K.; Takeoka, S.; Nishide, H.; Tsuchida, E. *Biotechnol. Prog.* **1996**, *12*, 119−125.

(10) Chung, T. W.; Huang, Y. Y.; Wu, C. I. *Artif. Cells. Blood Substitutes. Immobilization Biotechnol.* **1999**, *27*, 215−227.

(11) Nolte, D.; Pickelmann, S.; Lang, M.; Keipert, P.; Messmer, K. *Anesthesiology* **2000**, *93*, 1261−1270.

(12) Jouan-Hureaux, V.; Audonnet-Blaise, S.; Lacatusu, D.; Krafft, M. P.; Dewachter, P.; Cauchois, G.; Stoltz, J. F.; Longrois, D.; Menu, P. *Transfusion* **2006**, *46*, 1892−1898.

(13) Sakai, H.; Yuasa, M.; Onuma, H.; Takeoka, S.; Tsuchida, E. *Bioconjugate. Chem.* **2000**, *11*, 56−64.

(14) Vandegriff, K. D.; McCarthy, M.; Rohlfs, R. J.; Winslow, R. M. *Biophys. Chem.* **1997**, *69*, 23−30.

(15) Manjula, B. N.; Tsai, A.; Upadhya, R.; Perumalsamy, K.; Smith, P. K.; Malavalli, A.; Vandegriff, K.; Winslow, R. M.; Intaglietta, M.; Prabhakaran, M.; Friedman, M. J.; Acharya, A. S. *Bioconjugate Chem.* **2003**, *14*, 464−472.

10.1021/la7004503 CCC: $37.00 
Published on Web 06/13/2007

blood.[16,17] We reported previously that HbV suspended in plasma-derived HSA or rHSA was almost Newtonian: no aggregation was detected microscopically.[3,18] In Japan, rHSA will soon be approved for clinical use.[19] However, various plasma substitutes such as hydroxylethyl starch (HES), dextran (DEX), and modified fluid gelatin (MFG) are used worldwide.[20-22] The selection among these plasma substitutes should be determined not only by safety and efficacy but also by price, experience of clinicians, and customs of respective countries.

Water-soluble polymers generally interact with particles such as polystyrene beads, silica, liposomes, and red blood cells (RBCs) to induce aggregation or flocculation.[23-28] For that reason, it is important to determine the compatibility of HbV with these plasma substitutes. With that background, we studied the rheological properties of HbV suspended in these plasma substitute solutions for the first time using a complex rheometer and a microchannel array. This study provides a unique opportunity to investigate the rheology of a highly concentrated liposomal suspension.

## Materials and Methods

**Preparation of HbV.** The HbV used for this study was prepared by Oxygenix Co. Ltd. (Tokyo) under sterile conditions, as reported previously.[29-31] The Hb was purified from outdated donated blood provided by the Japanese Red Cross Society (Tokyo, Japan). The encapsulated purified Hb (38 g/dL) contained 14.7 mM pyridoxal 5′-phosphate (PLP; Sigma) as an allosteric effector at a molar ratio of PLP/Hb = 2.5. The lipid bilayer comprised a mixture of 1,2-dipalmitoyl-*sn*-glycero-3-phosphatidylcholine, cholesterol, and 1,5-bis-*O*-hexadecyl-*N*-succinyl-L-glutamate in a molar ratio of 5/5/1 (Nippon Fine Chemical Co. Ltd., Osaka, Japan) and 1,2-distearoyl-*sn*-glycero-3-phosphatidylethanolamine-*N*-poly(ethylene glycol) (NOF Corp., Tokyo, Japan, 0.3 mol % of the total lipid). The particle diameter was 279 ± 95 nm. The HbVs were suspended in a physiologic saline solution at [Hb] = 10 g/dL ([lipids] = ca. 6 g/dL) and were deoxygenated for storage with $N_2$ bubbling in vials.[32]

**Plasma Substitutes.** The plasma substitutes used in this study are listed in Table 1. Recombinant human serum albumin (rHSA, $M_w$ = 67 kDa, 25 wt %) was a gift from Nipro Corp. (Osaka, Japan). Before use, it was diluted to 5 wt % using saline solution (Otsuka Pharmaceutical Co. Ltd., Osaka, Japan). DEX solution ($M_w$ = 40 kDa, 10 wt % in a physiological saline solution) was purchased from Kobayashi Pharmaceutical Co. Ltd. (Osaka, Japan). An $HES_{70}$ solution (Saline-HES, $M_w$ = 68 kDa, 6 wt % in a physiological saline solution) was purchased from Kyorin Pharmaceutical Co. Ltd. (Osaka, Japan). An $HES_{130}$ solution (Voluven, $M_w$ = 130 kDa, 6 wt % in a physiological saline solution) and powdered $HES_{200}$ (HES200/0.5, $M_w$ = 200 kDa) were gifts from Fresenius Kabi AG (Homburg v.d.H., Germany). The $HES_{200}$ was dissolved in a physiological saline solution at 6 wt %. An $HES_{670}$ solution (Hextend, $M_w$ = 670 kDa, 6 wt % in a physiological Ringer lactate solution) was obtained from Hospira, Inc. (Lake Forest, IL). An MFG solution (Gelofusin, $M_w$ = 30 kDa, 4 wt % in a physiological saline solution) was a gift from B. Braun Melsungen AG (Melsungen, Germany). The COP was measured using a colloid osmometer (model 4420; Wescor, Inc., Logan, UT; molecular weight cutoff = 10 000).

**Table 1. Plasma-Substitute Solutions and Their Physicochemical Properties**[a]

| plasma-substitute solutions | $M_w$ (kDa) | $M_n$ (kDa) | $M_w/M_n$ | conc (g/dL) in saline | COP (Torr) | viscosity (mPa·s) at 25 °C at 10 $s^{-1}$ | viscosity (mPa·s) at 25 °C at 1000 $s^{-1}$ |
|---|---|---|---|---|---|---|---|
| DEX | 40[b] | 25[b] | 1.6 | 10[b] | 44 | 4.5 | 4.5 |
| MFG | 30[b] | 23[b] | 1.3 | 4[b] | 44 | 2.2 | 2.3 |
| $HES_{670}$ | 670[b] | 194[c] | 3.5 | 6[b] | 27 | 4.5 | 4.4 |
| $HES_{200}$ | 240[b] | 70[b] | 3.4 | 6 | 29 | 2.5 | 2.5 |
| $HES_{130}$ | 130[b] | 50[b] | 2.6 | 6[b] | 35 | 2.3 | 2.3 |
| $HES_{70}$ | 68[b] | 17[b] | 4.0 | 6[b] | 34 | 2.0 | 2.0 |
| rHSA | 67[b] | 67[b] | 1.0 | 5 | 19 | 1.3 | 1.2 |

[a] The viscosities at 10 and 1000 $s^{-1}$ are almost identical, indicating that these polymer solutions are Newtonian fluids. (See Supporting Information). DEX, dextran; HES, hydroxyethyl starch; MFG, modified fluid gelatin; rHSA, recombinant human serum albumin; COP, colloid osmotic pressure. [b] Data provided by the manufacturer. [c] Calculated from the concentration dependence of COP (unpublished data).

**Preparation of HbV Suspended in Plasma Substitutes and Blood Samples.** HbV suspended in a saline solution was ultracentrifuged (20 000*g*, 30 min) to produce HbV−particle sediment. After the removal of the upper saline solution, a plasma substitute solution was added, and the HbV was redispersed by stirring and vortexing; the final concentration was adjusted to [Hb] = 10 g/dL. Flocculation of HbV was apparent because HbV tended to phase separate and precipitate gradually when HbV was suspended either in $HES_{670}$, $HES_{200}$, $HES_{130}$, DEX, or MFG. However, the supernatant was transparent and not colored. Before rheological measurements, we measured the particle diameters using a light-scattering method (PCS submicron particle analyzer; Beckman Coulter Inc.) after diluting the flocculated HbV with a normal saline solution. The particle diameters (nm) of redispersed HbV (HbV-DEX, 270 ± 81; HbV-$HES_{670}$, 292 ± 101; and HbV-MFG, 278 ± 90) were almost identical to that of the original HbV suspension (279 ± 95 nm). These results indicate that no hemolysis occurred and that no morphological change in the individual HbV particles occurred. Immediately before measurement, the suspension was filtered (0.45 μm pore size, Dismic; Toyo Roshi Kaisha Ltd., Tokyo, Japan). For comparison, fresh human blood was withdrawn with heparinized syringes from three donors. Measurements were performed within 6 h after withdrawal.

**Viscoelastic Measurement of HbV Suspended in Plasma Substitutes.** Steady-shear viscosity and shear stress measurements, a strain−sweep measurement, and the step-shear rate procedure (relaxation test) were performed using a rheometer (Physica MCR 301; Anton Paar GmbH, Graz, Austria). The cone diameter was 50 mm; the gap angle between the cone and plate was 1°. A parallel plate (50 mm diameter) was also used to confirm the influence of the interface between the plates and the test materials. All measurements were performed at 25 °C. About 650 μL of the sample suspension was sandwiched between the cone and plate. The excess solution was wiped out. For the steady-shear viscosity measurement, the shear rate was decreased from $10^3$ to $10^{-4}$ $s^{-1}$. The shear rate was increased from $10^{-4}$ to $10^3$ $s^{-1}$ to confirm the presence of dynamic hysteresis. In this case, a preconditioning operation was performed for 60 s at 1 $s^{-1}$ and then standing still for 300 s. Some variance in the data was apparent at a lower shear rate, and the averaged viscosities and standard deviations are shown with the data ($n$ = 3).

(16) Sakai, H.; Masada, Y.; Horinouchi, H.; Yamamoto, M.; Ikeda, E.; Takeoka, S.; Kobayashi, K.; Tsuchida, E. *Crit. Care Med.* **2004**, *32*, 539−545.
(17) Yamazaki, M.; Aeba, R.; Yozu, R.; Kobayashi, K. *Circulation* **2006**, *114*, I220−I225.
(18) Sakai, H.; Tsai, A. G.; Kerger, H.; Park, S. I.; Takeoka, S.; Nishide, H.; Tsuchida, E.; Intaglietta, M. *J. Biomed. Mater. Res.* **1998**, *40*, 66−78.
(19) Kobayashi, K. *Biologicals* **2006**, *34*, 55−59.
(20) Webb, A. R.; Nash, G. B.; Dormandy, J. A.; Bennett, E. D. *Clin. Hemorheol.* **1990**, *10*, 287−296.
(21) Webb, A. R.; Barclay, S. A.; Bennett, E. D. *Intensive Care Med.* **1989**, *15*, 116−120.
(22) Traylor, R. J.; Pearl, R. G. *Anesth. Analg.* **1996**, *83*, 209−212.
(23) Meyuhas, D.; Nir, S.; Lichtenberg, D. *Biophys. J.* **1996**, *71*, 2602−2612.
(24) Sunamoto, J.; Iwamoto, K.; Kondo, H. *Biochem. Biophys. Res. Commun.* **1980**, *94*, 1367−1373.
(25) Otsubo, Y. *Langmuir* **1990**, *6*, 114−118.
(26) Tilcock, C. P.; Fisher, D. *Biochim. Biophys. Acta* **1982**, *688*, 645−652.
(27) Neu, B.; Meiselman, H. J. *Biophys. J.* **2002**, *83*, 2482−2490.
(28) Goto, Y.; Sakakura, S.; Hatta, M.; Sugiura, Y.; Kato, T. *Acta Anaesthesiol. Scand.* **1985**, *29*, 217−223.
(29) Takeoka, S.; Ohgushi, T.; Terase, K.; Ohmori, T.; Tsuchida, E. *Langmuir* **1996**, *12*, 1755−1759.
(30) Sou, K.; Naito, Y.; Endo, T.; Takeoka, S.; Tsuchida, E. *Biotechnol. Prog.* **2003**, *19*, 1547−1552.
(31) Sakai, H.; Masada, Y.; Takeoka, S.; Tsuchida, E. *J. Biochem. (Tokyo)* **2002**, *131*, 611−617.
(32) Sakai, H.; Tomiyama, K.; Sou, K.; Takeoka, S.; Tsuchida, E. *Bioconjugate Chem.* **2000**, *11*, 425−432.

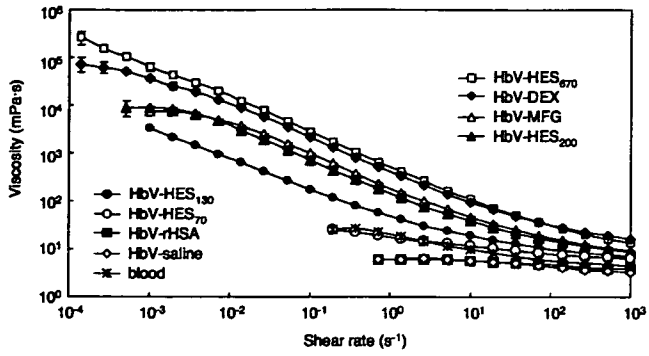


**Figure 1.** Viscosity of HbV suspended in various plasma-substitute solutions measured using an MCR 301 rheometer. The shear rate was decreased from $10^3$ to $10^{-4}$ $s^{-1}$. Fluids with higher viscosity were measurable at a lower shear rate because of a sufficiently high strain of detection. Therefore, the low-viscosity HbV-rHSA and HbV-saline were measurable only above 0.7 $s^{-1}$. [Hb] = 10 g/dL, 25 °C. The blood data are inserted for comparison. Mean ± SD ($n$ = 3).

Strain-sweep measurements were carried out in the strain range of 0.01−100% at a frequency of 2 Hz using the same cone-and-plate geometry.

For the step-shear rate procedure, the viscosity of the HbV suspension was measured continuously for 120 s at a shear rate of 0.1 $s^{-1}$ to confirm the constant viscosity. Next, the rotation speed of the cone plate was increased suddenly to attain a shear rate of 100 $s^{-1}$; this condition was maintained for 220 s. Subsequently, the rotational speed was lowered suddenly to attain a shear rate of 0.1 $s^{-1}$; this condition was maintained for 20 s. The response of the viscosity to the stepwise change of shear rates reflects the morphological change of HbV flocculation.

The respective dependencies of the storage modulus ($G'$), loss modulus ($G''$), and complex viscosity on the shear rate were analyzed using a dynamic capillary rheometer (DCR; Anton Paar GmbH) at shear rates of 5−330 $s^{-1}$ at 37 °C.[33]

**Microchannel Flow Measurement.** An array of microchannels (4.5 μm deep, 7 μm wide, 30 μm long, number 8736 in parallel, Bloody 6-7; Hitachi Haramachi Electronics Co. Ltd.) was used.[34] It was installed in a microchannel array flow analyzer (MC-FAN; Hitachi Haramachi Electronics Co. Ltd.). About 200 μL of the sample solution was inserted into the inlet syringe in order to flow through the microchannel array. The time necessary for a 100 μL suspension to pass through the channels at 20 $cmH_2O$, which corresponds to the capillary perfusion pressure, was measured ($n$ = 3). Microscopic images were made of the flow patterns and the flocculate formation under a static condition (shutoff).

## Results

**Viscosity and Shear Stress of HbV Suspended in Plasma Substitutes.** Figure 1 shows the viscosity of HbV suspended in various plasma substitute solutions when the shear rate decreased from $10^3$ to $10^{-4}$ $s^{-1}$. The HbV suspended in rHSA was a nearly Newtonian fluid; no remarkable difference existed between HbV-rHSA and HbV suspended in saline. The respective viscosities of HbV-rHSA and HbV-$HES_{70}$ were nearly equal to those of human blood in comparison with other combinations. Because of the detection limit of shear strain of this rheometer and the very low viscosity of HbV-rHSA, only measurements above 5 × $10^{-1}$ $s^{-1}$ were valid. However, HbV suspended in other polymer solutions—HES, DEX, and MFG—showed non-Newtonian properties with a high viscosity at lower shear rates, so-called

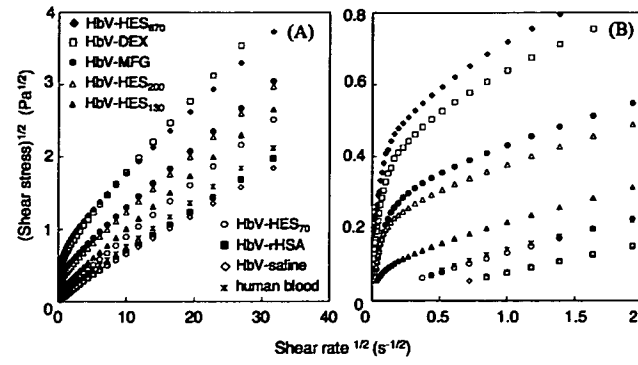


**Figure 2.** Casson plots of the square root of shear stress versus the square root of shear rate. These lines indicate that no clear stress yield exists. The graph is magnified in part B. Blood data are inserted for comparison.

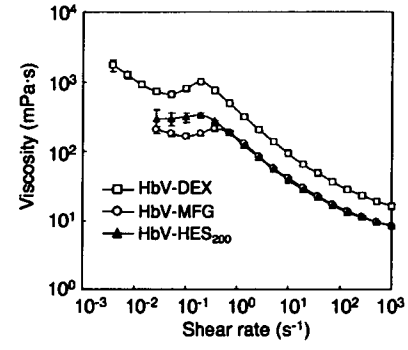


**Figure 3.** Shear thickening of HbV-DEX, HbV-$HES_{200}$, and HbV-MFG observed when the shear rate was increased in the opposite direction, from $10^{-4}$ to $10^3$ $s^{-1}$. [Hb] = 10 g/dL, 25 °C. Mean ± SD ($n$ = 3).

shear-thinning, attributable to the flocculate formation of HbV. The viscosities were measurable over a wider range of shear rates.

The series of different molecular weights of HES for HbV-HES reflected the molecular weight dependence of the viscosity: higher-molecular-weight HES displayed enhanced HbV flocculation.

As a comparative study, the shear rate dependencies of the viscosities of all of the plasma substitute solutions were measured. All solutions showed constant viscosities, indicating that they are all Newtonian fluids,[35−37] as shown in Table 1 and in Supporting Information.

Figure 2A,B shows Casson plots of shear stress versus the shear rate for all suspensions. HbV suspended in saline, rHSA, and $HES_{70}$ showed a relatively linear relationship. Other suspensions with high viscosities showed convex curves with marked deviations from the linear relationship, especially at lower shear rates. No stress yield is apparent for any line, even when the graph is magnified (Figure 2B).

Suspensions of HbV-DEX, HbV-$HES_{200}$, and HbV-MFG showed hysteresis of viscosity at lower shear rates (Figure 3) when the shear rate was changed in the opposite direction, from $10^{-4}$ to $10^3$ $s^{-1}$. In addition, a shoulder or a peak was visible at

(33) Thurston, G. B. *Biophys. J.* **1972**, *12*, 1205−1217.
(34) Kikuchi, Y.; Sato, K.; Mizuguchi, Y. *Microvasc. Res.* **1994**, *47*, 126−139.
(35) Tirtaatmadja, V.; Dunstan, D. E.; Boger, D. V. *J. Non-Newtonian Fluid Mech.* **2001**, *97*, 295−301.
(36) Corry, W. D.; Jackson, L. J.; Seaman, G. V. *Biorheology* **1983**, *20*, 705−717.
(37) Wulansari, R.; Mitchell, J. R.; Blanhard, J. M. V.; Paterson, J. L. *Food Hydrocolloids* **1998**, *12*, 245−249.
(38) Buscall, R.; Mills, P. D. A.; Goodwin, J. W.; Lawson, D. W. *J. Chem. Soc., Faraday Trans. 1* **1988**, *84*, 4249−4260.
(39) Chen, M.; Russel, W. B. *J. Colloid Interface Sci.* **1991**, *141*, 564−577.

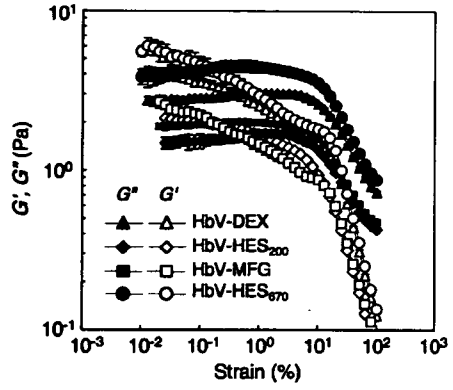


**Figure 4.** Strain dependence of the storage modulus ($G'$) and loss modulus ($G''$) of HbV suspended in various plasma substitutes. [Hb] = 10 g/dL, $f$ = 2 Hz. Mean ± SD ($n$ = 3).

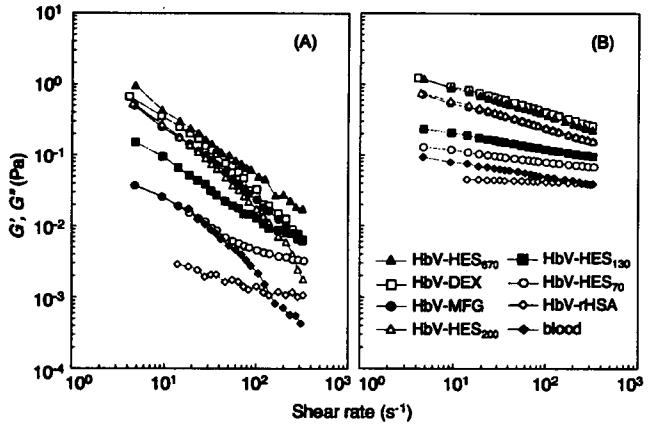


**Figure 5.** Respective shear rate dependencies of (A) the storage modulus, $G'$, and (B) the loss modulus, $G''$, of HbV suspended in various plasma-substitute solutions as measured using a DCR rheometer. [Hb] = 10 g/dL, 37 °C. The blood curves are shown for comparison.

around 0.1−1 $s^{-1}$, indicating the presence of shear thickening in this range. However, suspensions with lower viscosities—HbV-$HES_{70}$ and HbV-$HES_{130}$—showed a monotonous shear-thinning viscosity change (data not shown). Measurements with the parallel plate at different thicknesses of the suspensions also showed the shear-thickening effect (data not shown), indicating that this phenomenon is reproducible and unrelated to a skidding effect at the interface of the plate and the suspension.

**Measurement of the Storage Modulus ($G'$) and Loss Modulus ($G''$).** Figure 4 shows the strain dependence of the storage modulus ($G'$) and loss modulus ($G''$) at [Hb] = 10 g/dL, $f$ = 2 Hz. The elastic responses were predominant, producing higher $G'$ values than $G''$ values at lower strains for the highly flocculated HbV suspensions: HbV-DEX, HbV-$HES_{670}$, HbV-$HES_{200}$, and HES-MFG. The $G'$ value decreased gradually with increasing strain, but $G''$ was nearly constant at lower strains. Yielding points (critical strain $\gamma_c$) for these suspensions were at around 10% strain; in addition, the $\gamma_c$ values for the three samples were almost identical, irrespective of the different levels of $G''$. For HbV-rHSA, both $G'$ and $G''$ were too small to detect and were therefore not included in the Figure.

Figure 5 shows the shear rate dependency of $G'$ and $G''$ as measured using the capillary rheometer. At a lower shear rate, highly flocculated HbV suspensions HbV-DEX, $HES_{670}$-HbV, HbV-$HES_{200}$, and HbV-MFG showed high $G'$ values. The contribution of $G'$ decreased considerably when the HbV concentration was reduced at a constant polymer concentration.

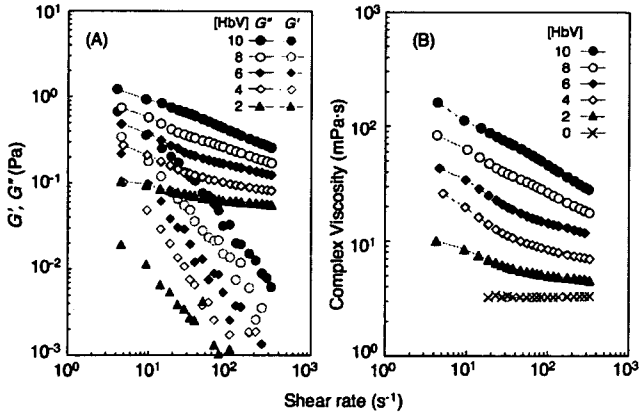


**Figure 6.** Representative profile of the concentration dependence (A) on $G'$ and $G''$ and (B) on complex viscosity when the concentration of HbV in HbV-DEX was reduced from [Hb] = 10 to 0 g/dL at a constant DEX concentration (10 g/dL).

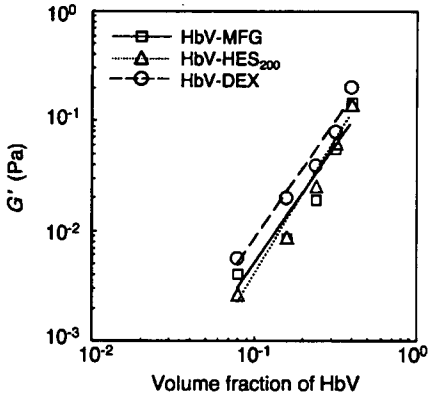


**Figure 7.** Logarithmic plots of $G'$ at 18 $s^{-1}$ vs $\phi$ (volume fraction of HbV) for HbV-DEX, HbV-$HES_{200}$, and HbV-MFG. For all cases, $G'$ varies with $\phi$ following a power law of order 2.1−2.4. HbV-DEX, $G'-\phi^{2.13}$ ($R^2$ = 0.9722); HbV-HES, $G'-\phi^{2.45}$ ($R^2$ = 0.9753); and HbV-MFG, $G'-\phi^{2.14}$ ($R^2$ = 0.9139).

Figure 6A shows a representative profile of HbV-DEX at a constant dextran concentration. The complex viscosity of HbV-DEX depends strongly on the concentration of HbV (**Figure 6B**). For example, the complex viscosity at 320 $s^{-1}$ decreased from 28 to 5 mPa·s when the Hb concentration decreased from 10 to 2 g/dL. Other plasma substitutes displayed similar profiles (data not shown).

The relationship between $G'$ and $\phi$ (volume fraction of HbV) provides important information about the nature of particle flocculation.[35,36] Figure 7 shows a logarithmic graph of $G'$ at 18 $s^{-1}$ versus $\phi$ for HbV-DEX, HbV-$HES_{200}$, and HbV-MFG. Those graphs show an almost linear relationship: $G'$ varies with $\phi$, following a power law of order 2.1−2.4.

**Relaxation Test of HbV Suspended in Plasma Substitutes.** Figure 8A shows the response of viscosity to the rapid change of the shear rate. At a low shear rate (0.1 $s^{-1}$), the suspensions of HbV-DEX, HbV-$HES_{670}$, HbV-$HES_{200}$, and HbV-MFG showed very high viscosities because of flocculation. The viscosities decreased rapidly when the shear rate increased rapidly to 100 $s^{-1}$ (which corresponds to the shear rate in a venule). The viscosities returned spontaneously to the original levels when the shear rate reverted rapidly to 0.1 $s^{-1}$. Figure 8B shows a magnification of the data for jumping points of Figure 8A, which clarifies that the suspension responded very promptly to the change in the shear rate. The reduction of viscosities that corresponded to the dissociation of flocculation was completed within 0.2 s,

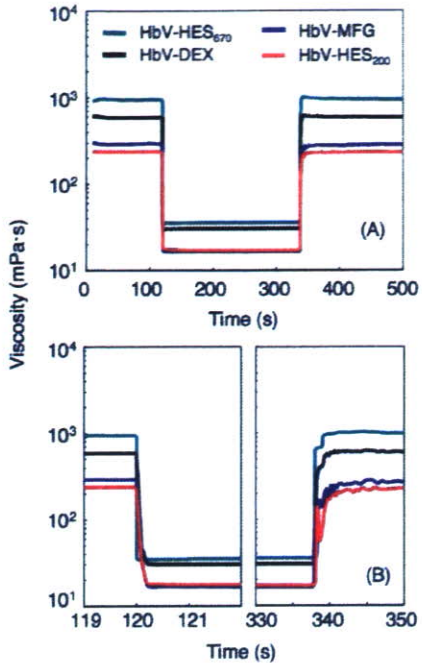


**Figure 8.** (A) Response of the viscosity of HbV suspended in DEX, $HES_{200}$, $HES_{670}$, and MFG to the rapid change in shear rate as measured using the MCR 301 rheometer. The shear rate changed rapidly from 0.1 to 100 $s^{-1}$; it then returned to 0.1 $s^{-1}$. The graph is magnified in B. [Hb] = 10 g/dL, 25 °C.

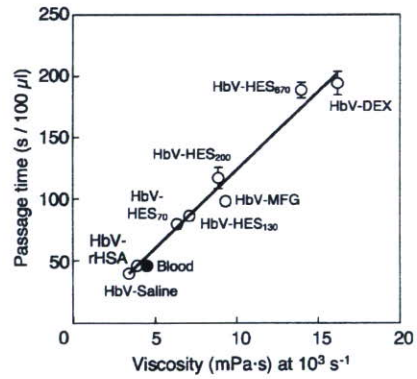


**Figure 9.** Microchannel flow measurements of HbV suspended in various plasma-substitute solutions and human blood. The time required for the passage of 100 $\mu$L of each suspension was plotted against the viscosity at 1000 $s^{-1}$ (from Figure 1). The straight line indicates a linear approximation: $Y = 12.4X$ ($R^2 = 0.9727$). Mean ± SD ($n = 3$).

and the recovery of viscosity that corresponded to flocculate formation was completed within 2 s. Although the responses should depend partially on the sharpness of the shear rate change induced by the motion of the cone plate, these data indicate that the flocculation of HbV is formed rapidly by weak interaction and that it is completely reversible.

**Microchannel Flow Measurement.** Figure 9 summarizes the relationship between the viscosity of the HbV suspensions at a shear rate of $10^3$ $s^{-1}$ and the time required for the passage of 100 $\mu$L of the suspensions through the microchannels. The most viscous HbV-DEX required the longest time: 194 ± 10 s. Apparently, a proportional relationship exists between the time required for passage and the fluid viscosity ($R^2 = 0.9727$).

Despite the high viscosities of HbV-DEX, HbV-$HES_{670}$, HbV-MFG, and HbV-$HES_{200}$, microscopic observation indicated that no plugging of the microchannels occurred under the flow

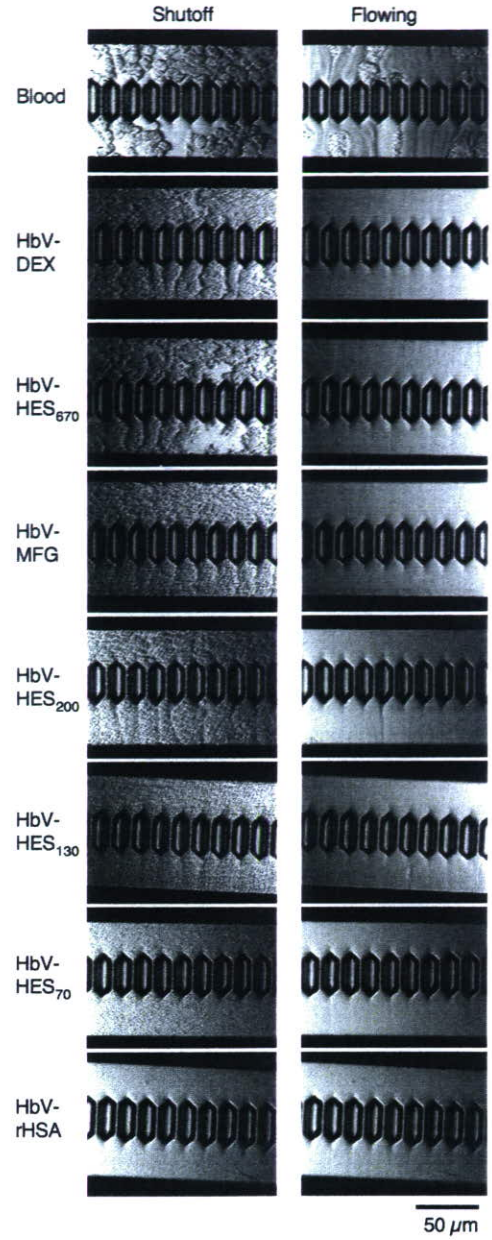


**Figure 10.** Images of microchannels during the flowing condition and at flow cessation. The direction of flow is from top to bottom. Flocculate formation is apparent at cessation for HbV-DEX, HbV-HES, and HbV-MFG. However, no flocculation was apparent for HbV-rHSA. Under the flowing condition, no plugging of channels occurred for any HbV suspension. However, blood showed partial plugging. In the HES series, a higher-molecular-weight HES shows larger flocculation at cessation.

condition even though clear flocculate formation existed for the cessation of flow (Figure 10). However, stored blood showed the partial plugging of channels even though its viscosity (4.5 mPa·s) and the time required for passage (48 s) were much less than that for HbV suspended in other polymer solutions. At shutoff, HbV-DEX, HbV-MFG, HbV-$HES_{200}$, and HbV-$HES_{670}$ showed traces of channel flow and phase separation of the suspending medium and flocculation.

## Discussion

The results of this study clarified that the HbV suspension has a unique rheological profile from the viewpoint of "suspension rheology." Liposomes are well known to form flocculates or

aggregates in the presence of water-soluble polymers[23,24,40] that were analyzed mainly by turbidity or light-scattering measurements at a very low concentration, where a suspension would consist of a collection of discrete flocculates. However, the HbV suspension consists of a high concentration of HbV with a weight fraction of nearly 16 g/dL in all and a volume fraction of about 40 vol %. Therefore, the flocculated HbV would respond elastically to small deformations, as indicated by the considerable increase in the storage modulus ($G'$) of flocculated suspensions.[25,41] The rheometer that we used (Physica MCR 301) is extremely sensitive to slight shear stress, thereby enabling the detection of subtle rheological changes over a wide range of shear rates ($10^{-4}-10^{3}\ s^{-1}$). The RBCs are well known to aggregate reversibly; they are a determinant of the viscoelastic property of non-Newtonian blood because they occupy 40−55% of the blood volume.[33,42] The RBC aggregation, induced by the addition of a water-soluble polymer, influences blood viscosity, hemodynamics, and tissue oxygenation.[43−46] Therefore, it is important to determine the rheological profiles of HbV suspensions as a transfusion alternative.

The HbV suspended in rHSA, a globular protein solution, was a nearly Newtonian fluid. The level of viscosity at higher shear rates was nearly equal to that of human blood. In contrast, HbV suspended in other polymer solutions—HES, DEX, and MFG—showed non-Newtonian properties with a high viscosity at a lower shear rate (shear thinning) because of the flocculation of HbV. A series of HES solutions showed a clear molecular-weight dependence for inducing flocculation. In addition, HbV-$HES_{70}$ showed a similar curve to that of blood. For all combinations of HbV and a polymer solution, the flocculation of HbV should be dissociated at a higher shear rate. Interestingly, the Casson plots show no stress yield for any suspension, probably because the rheometer that we used can measure shear stress values successively, even at extremely low shear rates of $10^{-4}\ s^{-1}$. It is speculated that flocculation formation and dissociation are successive and that no marked critical point exists.

The mechanism of liposome flocculation remains controversial. It is well established in our laboratory that intermacromolecular interactions in water solutions produce macromolecular complexes such as a polyelectrolyte complex and a hydrogen-bonding complex.[47] Therefore, it was plausible that (i) polymer chains would adsorb onto the surfaces of the particles directly to produce bridges.[24] However, it is well known that a PEG aqueous solution and a polysaccharide aqueous solution are immiscible, and it cannot explain the adsorption of DEX and HES on the surface of PEG-modified HbV. Another mechanism was that (ii) the hydration of polymer chains would deflect water molecules from the particles and thereby exclude the particles from the bulk solution.[26] However, this was denied by Meyuhas et al.[23] by the fact that dialysis of liposomes against polymer-containing solutions did not induce aggregation whereas direct addition of the polymer to the liposome solution induced flocculation. Recent practical and theoretical analyses contradict these theories and suggest a depletion mechanism: (iii) A depletion layer develops near a particle surface that is in contact with a polymer solution if the loss of configurational entropy of the polymer coil is not balanced by adsorption energy. Within this layer, the polymer concentration is lower than in the bulk phase. Consequently, as particles approach, the osmotic pressure difference between the interparticle polymer-poor depletion layer and the bulk phase results in solvent displacement into the bulk phase and depletion interaction. Because of this interaction, an attractive force of particles tends to minimize the polymer-poor space between the particles, thereby inducing flocculation.[23,27,48,49]

In the case of depletion interaction, the size of the polymer coil in comparison to interparticle spacing is important. Macromolecules of HES, DEX, and MFG should contain branches; the polymers are more extended or linear than the globular, compact structure of HSA.[50] According to the literature, the radii of gyration ($R_g$) of these polymers are estimated to be $HES_{670}$ (ca. 19.7 nm), $HES_{130}$ (ca. 12.3 nm),[51] DEX (ca. 8.1 nm),[52] MFG (ca. 10.7 nm);[53] and HSA with the smallest value (ca. 2.8 nm).[54] Even though the $R_g$ of MFG is only half that of $HES_{670}$, the molar concentration of MFG (1.7 mM), calculated from the concentration and $M_n$, is about 6 times larger than that of $HES_{670}$ (0.3 mM). It is probable that the more extended polymer chains and the higher molar concentration enhance the exclusion effect from the hydrated sphere of the vesicles, creating a more flocculated vesicle structure. One limitation of this study is that we selected the clinically approved polymer solutions only from a practical point of view. Therefore, the molecular weight distributions are very wide, as indicated by their large $M_w/M_n$ ratios, and their molar concentrations are different. Further analyses are ongoing to clarify the flocculation mechanism using polymers with strictly defined molecular weights and concentrations.

Interestingly, we observed dynamic hysteresis and a shear-thickening profile when the shear rate was increased in the opposite direction for suspensions that showed very high viscosities (HbV-DEX, HbV-$HES_{670}$, HbV-$HES_{200}$, and HbV-MFG). These results indicate that the rheological properties of these suspensions are influenced by the time history of the suspension for the growth of flocculation. Typical shear thickening is reported in the case of styrene-methyl acrylate copolymer particles mixed with poly(acrylic acid),[55] which is attributable to the nonlinear elasticity resulting from the entropy of extended bridges and forced desorption caused by hydrodynamic effects. For HbV suspensions, it is speculated that a higher shear rate would extend the distance separating the HbV particles, causing an entropy loss of the solution of polymers with larger $R_g$, which would cause a regional shear-thickening effect. Another reason would be related to the sedimentation of flocculated HbV, even in the thin solution between the cone and plate. In this case, the concentration of HbV would be lower at the upper layer near the cone, resulting in a slightly lower viscosity at a lower shear rate. With increasing shear rate, the suspension would be homogenized, showing a higher viscosity as a shoulder in Figure 3.

(40) Sou, K.; Endo, T.; Takeoka, S.; Tsuchida, E. *Bioconjugate Chem.* **2000**, *11*, 372−379.
(41) Otsubo, Y. *Heterogeneous Chem. Rev.* **1996**, *3*, 327−349.
(42) Chien, S.; King, R. G.; Skalak, R.; Usami, S.; Copley, A. L. *Biorheology* **1975**, *12*, 341−346.
(43) Freyburger, G.; Dubreuil, M.; Boisseau, M. R.; Janvier, G. *Br. J. Anaesth.* **1996**, *76*, 519−525.
(44) Eckmann, D. M.; Bowers, S.; Stecker, M.; Cheung, A. T. *Anesth. Analg.* **2000**, *91*, 539−545.
(45) Bishop, J. J.; Nance, P. R.; Popel, A. S.; Intaglietta, M.; Johnson, P. C. *Am. J. Physiol. Heart Circ. Physiol.* **2001**, *280*, H222−H236.
(46) Tateishi, N.; Suzuki, Y.; Cicha, I.; Maeda, N. *Am. J. Physiol. Heart Circ. Physiol.* **2001**, *281*, H448−H456.
(47) Tsuchida, E.; Abe, K. *Adv. Polym. Sci.* **1982**, *45*, 1−119.
(48) Neu, B.; Meiselman, H. J. *Biochim. Biophys. Acta* **2006**, *1760*, 1772−1779.
(49) Vincent, B.; Edwards, J.; Emmett, S.; Jones, A. *Colloids Surf.* **1986**, *18*, 261−281.
(50) Takaori, M.; Kobori, M. *Plasma Substitutes and Their Clinical Use*; Kokuseido Publisher: Tokyo, 2004.
(51) Gosch, C. I.; Haase, T.; Wolf, B. A.; Kulicke, W. *Starch* **2002**, *54*, 375−384.
(52) Hirata, Y.; Sano, Y.; Aoki, M.; Shohji, H.; Katoh, S.; Abe, J.; Hitsukuri, S.; Yamamoto, H. *Carbohydr. Polym.* **2003**, *53*, 331−335.
(53) Kaur, M.; Jumel, K.; Hardie, K. R.; Hardman, A.; Meadows, J.; Melia, C. D. *J. Chromatogr., A* **2002**, *957*, 139−148.
(54) Almogren, A.; Furtado, P. B.; Sun, Z.; Perkins, S. J.; Kerr, M. A. *J. Mol. Biol.* **2006**, *356*, 413−431.
(55) Otsubo, Y. *Langmuir* **1999**, *15*, 1960−1965.

The elastic properties of the HbV suspension are readily apparent from the high contribution of the storage modulus ($G'$). In fact, $G'$ was higher for more viscous HbV suspensions, such as HbV-DEX, HbV-$HES_{200}$, and HbV-MFG. The strain−sweep measurement clarified that $G'$ decreased gradually with increasing strain. However, $G''$ was nearly constant at lower strains, and the yielding point for these suspensions was as high as 10% strain. These results indicate that the HbV flocculation structure is not rigid and that reformation occurs easily with subtle strain.

It is speculated that the flocculation of HbV includes interconnected fractal clusters. As shown in Figure 6, both $G'$ and the viscosity increase with increasing concentration of HbV. The logarithmic graph of $G'$ versus $\phi$ (volume fraction of HbV) shows an almost linear relationship. A theory of Bascall et al.[38] for networks consisting of interconnected fractal clusters predicts $G'-\phi^{3.5\pm0.2}$ for diffusion-limited flocculation and $G'-\phi^{4.5\pm0.2}$ for chemically limited aggregation.[39] For the HbV suspensions, $G'$ varies with $\phi$ following a power law of order 2.1−2.4 and is much smaller than the theoretical values, supporting the idea that HbV forms fractal clusters through a very weak interaction and that diffusion-limited flocculation is plausible. This also supports the idea that polymer adsorption on the surface of HbV would not involve this system and that the weak interaction enables reversible and rapid flocculation−dissociation in response to the rapid change in shear rates, as shown in Figure 8, and the high yielding point of the stress−sweep measurement in Figure 4.

We reported previously that the surface modification of HbV with PEG prevents aggregation in an HSA solution.[3,18] The amount of PEG is sufficient to prevent aggregation formation in plasma. However, results of the present study show that, even with the PEG modification, HbV undergoes flocculation or aggregation when dispersed into a series of plasma substitutes. Notwithstanding, the flocculation seems not to plug the capillaries, as demonstrated for the first time by microchannel flow experiments. Under a static condition, microscopic observation clearly revealed flocculation. Under the flowing condition in the microchannels, visual observation confirmed the flocculation. However, no plugging was detected in the channels. The time necessary for passage at a perfusion pressure of 20 $cmH_2O$, which corresponded to an in vivo capillary pressure, was proportional to the fluid viscosity, according to Poiseuille's theory at constant pressure. However, the time required for the passage of blood should depend on the deformability of red blood cells and the activation of platelets and white cells, depending on a pathological condition.[34]

In a living body, perfusion pressure, vascular resistance, and blood viscosity determine organ blood flow. According to Poisseuille's law, increased viscosity reduces flow at a constant applied pressure. For the substitution of a large volume of blood with an HbV suspension as a "transfusion alternative", HbV-rHSA and HbV-$HES_{70}$ with similar viscosity to that of human blood would apparently be appropriate to maintain blood rheology and systemic hemodynamics. It remains to be examined whether other viscous combinations of HbV with DEX, higher-molecular-weight HES, and MFG would be acceptable to a living body. A possible utilization of HbV would be injection at a perioperative hemorrhage. A plasma substitute solution would be injected in an initial phase to maintain blood volume, causing hemodilution, followed by the injection of HbV to maintain $O_2$ content. This procedure would cause the dilution of both the plasma substitute and HbV. Therefore, the level of HbV flocculation and the viscosity would be reduced somewhat. Actually, we conducted the isovolemic hemodilution of 60% blood volume of rats with the series of plasma substitute solutions and subsequent injection of HbV. The results showed that systemic hemodynamic and respiratory functions were preserved and that no effect of flocculation was evident (unpublished data). The details will be reported elsewhere.

From a physiological point of view, changes in blood viscosity are accompanied by changes in vascular geometry because of autoregulatory processes that are driven by changes in the production of endothelium-derived vasorelaxation factors such as nitric oxide and prostacyclin in response to shear stress on the vascular wall.[56] Progressive hemodilution with a plasma substitute solution decreases blood viscosity, thereby increasing blood flow and vasoconstriction.[57] However, a viscous fluid is advantageous for imparting shear stress on the vascular wall to facilitate the production of vasorelaxation factors and thereby enhance vasorelaxation to improve peripheral blood flow. High blood viscosity is advantageous for transmitting pressure homogeneously to the microvascular network and thereby supplying blood to all capillaries.[58−60] A high-molecular-weight dextran-induced hyperviscosity of blood engenders the dilation of blood vessels.[61] Hemoconcentration increases blood viscosity but reduces vascular resistance.[62] Actually, Erni et al. tested the 40% blood exchange transfusion with HbV suspended in DEX and $HES_{200}$; they found no capillary plugging. They did find increased plasma viscosity and an improvement of microcirculatory blood flow in ischemic tissues in a hamster skin-flap model.[63−65]

In conclusion, the rheological property of HbV suspension is adjustable to that of human blood through the combination of rHSA and $HES_{70}$. Other plasma substitutes, such as high-molecular-weight HES, DEX, and MFG, cause HbV flocculation and hyperviscosity. However, reports show that hyperviscosity would not necessarily cause deterioration and in some cases might be advantageous to the body. The combination of HbV and plasma substitute solutions provides a unique opportunity to manipulate the suspension rheology not only as a transfusion alternative but also for other clinical applications such as the oxygenation of ischemic tissues and the ex vivo perfusion system. Further research is necessary to clarify the mechanism of flocculation and the in vivo safety of the combination of HbV and various kinds of plasma substitutes. Projects to collect such data are under way.

**Acknowledgment.** We acknowledge Dr. Masuhiko Takaori (East Takarazuka Satoh Hospital), Dr. Amy G. Tsai (University of California, San Diego), and Dr. Dominique Erni (Inselspital Hospital, University of Bern) for meaningful discussions related to plasma substitutes and Professor Yasufumi Otsubo (Chiba University) and Mr. N. Hirano (Nihon SiberHegner K.K., Tokyo)

(56) Smiesko, V.; Johnson, P. C. *News Physiol. Sci.* **1993**, *8*, 34−38.
(57) Hudak, M. L.; Jones, M. D., Jr.; Popel, A. S.; Koehler, R. C.; Traystman, R. J.; Zeger, S. L. *Am. J. Physiol. Heart Circ. Physiol.* **1989**, *257*, H912−H917.
(58) Tsai, A. G.; Acero, C.; Nance, P. R.; Cabrales, P.; Frangos, J. A.; Buerk, D. G.; Intaglietta, M. *Am. J. Physiol. Heart Circ. Physiol.* **2005**, *288*, H1730−H1739.
(59) Tsai, A. G.; Intaglietta, M. *Biorheology* **2001**, *38*, 229−237.
(60) de Wit, C.; Schafer, C.; von Bismarck, P.; Bolz, S. S.; Pohl, U. *Pflugers Arch.* **1997**, *434*, 354−361.
(61) Chen, R. Y. Z.; Carlin, R. D.; Simchon, S.; Jan, K. M.; Chien, S. *Am. J. Physiol. Heart Circ. Physiol.* **1989**, *256*, H898−H905.
(62) Martini, J.; Tsai, A. G.; Cabrales, P.; Johnson, P. C.; Intaglietta, M. *Am. J. Physiol. Heart Circ. Physiol.* **2006**, *291*, H310−H317.
(63) Plock, J. A.; Contaldo, C.; Sakai, H.; Tsuchida, E.; Leunig, M.; Banic, A.; Menger, M. D.; Erni, D. *Am. J. Physiol. Heart Circ. Physiol.* **2005**, *289*, H2624−H2631.
(64) Contaldo, C.; Plock, J.; Sakai, H.; Takeoka, S.; Tsuchida, E.; Leunig, M.; Banic, A.; Erni, D. *Crit. Care Med.* **2005**, *33*, 806−812.
(65) Contaldo, C.; Schramm, S.; Wettstein, R.; Sakai, H.; Takeoka, S.; Tsuchida, E.; Leunig, M.; Banic, A.; Erni, D. *Am. J. Physiol. Heart Circ. Physiol.* **2003**, *285*, H1140−1147.

for discussions of technical problems pertaining to viscoelastic measurements. The rHSA, HES, and MFG used in this study were gifts from Nipro Co., Fresenius Kabi A.G., and B. Braun, respectively. This study was supported by Health and Labour Sciences Research Grants (Research on the Regulatory Science of Pharmaceuticals and Medical Devices), the Ministry of Health, Labour and Welfare, Japan (H.S., E.T.). Grants-in-Aid for Scientific Research from the Japan Society for the Promotion of Science (B16300162) (H.S.), and Oxygenix Inc. (Tokyo, Japan). H.S., S.T., and E.T. are consultants of Oxygenix Inc.

**Supporting Information Available:** Viscosity of plasma-substitute solutions. This material is available free of charge via the Internet at http://pubs.acs.org.

LA7004503

THE JOURNAL OF BIOLOGICAL CHEMISTRY VOL. 283, NO. 3, pp. 1508–1517, January 18, 2008


# Encapsulation of Concentrated Hemoglobin Solution in Phospholipid Vesicles Retards the Reaction with NO, but Not CO, by Intracellular Diffusion Barrier*

Received for publication, September 12, 2007, and in revised form, November 13, 2007 Published, JBC Papers in Press, November 14, 2007, DOI 10.1074/jbc.M707660200

**Hiromi Sakai[‡], Atsushi Sato[§], Kaoru Masuda[¶], Shinji Takeoka[§1], and Eishun Tsuchida[‡2]**

*From the [‡]Research Institute for Science and Engineering and [§]Graduate School of Advanced Science and Engineering, Waseda University, Tokyo 169-8555, Japan and [¶]Kobelco Research Institute, Inc., Kobe 651-2271, Japan*

**One physiological significance of the red blood cell (RBC) structure is that NO binding of Hb is retarded by encapsulation with the cell membrane. To clarify the mechanism, we analyzed Hb-vesicles (HbVs) with different intracellular Hb concentrations, $[Hb]_{in}$, and different particle sizes using stopped-flow spectrophotometry. The apparent NO binding rate constant, $k'_{on}{}^{(NO)}$, of HbV at $[Hb]_{in}$ = 1 g/dl was 2.6 × $10^7$ $M^{-1}$ $s^{-1}$, which was almost equal to $k_{on}{}^{(NO)}$ of molecular Hb, indicating that the lipid membrane presents no obstacle for NO binding. With increasing $[Hb]_{in}$ to 35 g/dl, $k'_{on}{}^{(NO)}$ decreased to 0.9 × $10^7$ $M^{-1}$ $s^{-1}$, which was further decreased to 0.5 × $10^7$ $M^{-1}$ $s^{-1}$ with enlarging particle diameter from 265 to 452 nm. For CO binding, which is intrinsically much slower than NO binding, $k'_{on}{}^{(CO)}$ did not change greatly with $[Hb]_{in}$ and the particle diameter. Results obtained using diffusion simulations coupled with elementary binding reactions concur with these tendencies and clarify that NO is trapped rapidly by Hb from the interior surface region to the core of HbV at a high $[Hb]_{in}$, retarding NO diffusion toward the core of HbV. In contrast, slow CO binding allows time for further CO-diffusion to the core. Simulations extrapolated to larger particles (8 μm) showing retardation even for CO binding. The obtained $k'_{on}{}^{(NO)}$ and $k'_{on}{}^{(CO)}$ yield values similar to those reported for RBCs. In summary, the intracellular, not extracellular, diffusion barrier is predominant due to the rapid NO binding that induces a rapid sink of NO from the interior surface to the core, retarding further NO diffusion and binding.**

Physicochemical analyses of $O_2$ uptake and release behaviors of red blood cells (RBCs)[3] have revealed that the cellular structure retards all reactions in comparison with the homogeneous cell-free Hb solution (1–5). However, nature has selected this cellular structure through evolution. Reasons for Hb encapsulation in RBCs are as follows: (i) decreases in a high colloidal osmotic pressure of an Hb solution; (ii) prevention of removal of Hb from blood circulation through renal gloreruli; (iii) preservation of the chemical environment in cells, such as the concentrations of electrolytes (phosphates, 2,3-diphosphoglyceric acid, ATP, etc.) and many enzymes; and (iv) modulation of entrapment of endogenous gaseous messenger molecules (NO and CO) (6, 7) because it has been clarified in pathological conditions with hemolysis (8) and in the development of some Hb-based oxygen carriers (HBOCs) (9–16) that entrapment of endothelium-derived NO induces vasoconstriction, hypertension, reduced blood flow, and vascular damage. CO is also a vasorelaxation factor, especially in hepatic microcirculation (17). Entrapment of CO by a cell-free Hb solution induces constriction of sinusoidal capillaries (18). These side effects of molecular Hb imply the importance of the cellular structure of RBC.

Despite such a background in this field, the mechanism of retardation of NO binding by Hb encapsulation in RBC remains controversial (19–21). It remains unclear whether (i) an unstirred layer is formed as an extracellular diffusion barrier surrounding the RBC (6, 9); (ii) a protein-rich RBC cytoskeletal submembrane becomes a physical barrier against NO diffusion (22, 23); or (iii) gas diffusion is retarded because of the viscous Hb solution in RBC (2). As chemists, it seems to us that these controversies are attributable to the complex and fragile structure of RBC and chemically unstable NO, which make it difficult to analyze the binding rate constant of NO to RBC.

Hemoglobin-vesicles (HbVs) or liposome- encapsulated Hbs have been developed as transfusion alternatives. Their efficacy as $O_2$ carriers is comparable with that of RBC (24–28). It has been thought that liposomes as a molecular assembly are a fragile capsule. However, appropriate lipid composition and polyethylene glycol modification on the surface of vesicles stabilize the dispersion state (29) and enable stopped-flow measure-

* This work was supported in part by Health and Labor Sciences Research Grants (Research on Regulatory Science of Pharmaceuticals and Medical Devices), Ministry of Health, Labor, and Welfare, Japan (to H. S. and E. T.) and by Grants-in-Aid for Scientific Research from the Japan Society for the Promotion of Science B16300162 (to H. S.) and 18500368 (to S. T.), and Global COE "Practical Chemical Wisdom" (to S. T.). The costs of publication of this article were defrayed in part by the payment of page charges. This article must therefore be hereby marked "*advertisement*" in accordance with 18 U.S.C. Section 1734 solely to indicate this fact.

[1] Present address: Consolidated Research Institute for Advanced Science and Medical Care, Waseda University, 3-4-1 Okubo, Shinjuku, Tokyo 169-8555, Japan.

[2] To whom correspondence should be addressed: Research Institute for Science and Engineering, Waseda University, 3-4-1 Okubo, Shinjuku, Tokyo 169-8555, Japan. Tel.: 81-3-5286-3120; Fax: 81-3-3205-4740; E-mail: eishun@waseda.jp.

[3] The abbreviations used are: RBC, red blood cell; Hb, hemoglobin; metHb, methemoglobin; deoxyHb, deoxyhemoglobin; HbV, hemoglobin-vesicles; $[Hb]_{in}$, intracellular Hb concentration; $[heme]_{in}$, intracellular heme concentration; $k_{on}$, binding rate constant of elementary reaction; $k'_{on}{}^{(NO)}$, apparent NO binding rate constant; $k'_{on}{}^{(CO)}$, apparent CO binding rate constant; HBOC, Hb-based oxygen carrier; $P_{50}$, oxygen partial pressure at which Hb is half-saturated; $D_{Hb}$, diffusion constant of Hb; $D_{O_2}$, diffusion constant of $O_2$; $D_{NO}$, diffusion constant of NO; $D_{CO}$, diffusion constant of CO.

ments without causing hemolysis (26, 30). Although stopped-flow measurement is becoming classical, it allows accurate measurement of the binding rate constant of ligands (31). HbV is a molecular assembly composed of lipids and a concentrated Hb solution (32), and its physicochemical properties can be regulated easily (33–35) to elucidate their influences on the ligand binding profiles. In this paper, we describe analyses of the influences of intracellular Hb concentration, $[Hb]_{in}$, and the particle size of HbV on the apparent binding rate constants of NO and CO. Moreover, we attempted computer simulations to recreate the phenomena, clarify the underlying mechanism, and predict the ligand binding profiles of larger particles, such as RBCs.

**TABLE 1**

**Physicochemical characterization of a series of HbV prepared for the stopped flow spectrophotometry to observe the NO and CO binding profiles**

Samples 1–4 were used to examine the influence of intracellular Hb concentration ($[Hb]_{in}$). Samples 4–6 were used to study the influence of particle diameter. The $P_{50}$ value (oxygen tension at which Hb is half-saturated with oxygen) were regulated in the narrow range of 13–16 torrs to minimize the influence of Hb allostery on the binding rate constants of NO and CO.

| Sample entry number | $[Hb]_{in}$ | Particle size | $P_{50}$ |
|---|---|---|---|
| | *g/dl* | *nm* | *torrs* |
| 1 | 1 | 305 ± 105 | 13 |
| 2 | 10 | 277 ± 103 | 15 |
| 3 | 20 | 278 ± 94 | 15 |
| 4 | 35 | 265 ± 57 | 14 |
| 5 | 35 | 178 ± 74 | 16 |
| 6 | 35 | 452 ± 184 | 14 |

## EXPERIMENTAL PROCEDURES

*Preparation of Hb Solution and Hb-vesicles with Various $[Hb]_{in}$*—A concentrated human carbonylhemoglobin solution (40 g/dl, desalted) was obtained through purification from outdated donated blood provided by the Japanese Red Cross Society (Tokyo, Japan), as reported previously (36, 37). This was diluted by 10 times with a phosphate-buffered saline (PBS) solution (pH 7.4; Wako Pure Chemical Industries Ltd., Tokyo). It was then concentrated again to 40 g/dl using an ultrafiltration (cut-off $M_r$ 10,000; Advantec, Tokyo) at 4 °C. This solution was diluted to 1, 10, 20, and 35 g/dl using the same PBS solution. They were used for preparation of HbV with different $[Hb]_{in}$. The viscosities of these Hb solutions were measured using a rheometer (Physica MCR 301; Anton Paar GmbH, Graz, Austria) as 0.9, 1.1, 2.1, and 10.1 centipose, respectively, at 10 $s^{-1}$ and 25 °C. In this experiment, we added no allosteric effector, such as an organic phosphate, because we intended to compare the Hb solution and HbV with different $[Hb]_{in}$ at the same $O_2$ affinity ($P_{50}$, oxygen partial pressure at which Hb is half-saturated). A linear relationship exists between $P_{50}$ and NO affinity of Hb (38). In the present study, $P_{50}$ was regulated solely using $Cl^-$ and phosphate of PBS (35). The lipid bilayer comprised 1,2-dipalmitoyl-*sn*-glycero-3-phosphatidylcholine, cholesterol, 1,5-*O*-dihexadecyl-*N*-succinyl-L-glutamate (Nippon Fine Chemical Co. Ltd., Osaka, Japan), and 1,2-distearoyl-*sn*-glycerol-3-phosphatidylethanolamine-*N*-polyethylene glycol 5000 (NOF Corp., Tokyo, Japan) at a molar composition of 5/5/1/0.033. It is reported that unsaturated phospholipids are susceptible to lipid peroxidation and induce Hb denaturation (39, 40). Hb interacts with such a liposomal membrane and converts to metHb, leading synergistically to the heme loss and lipid peroxidation. Unsaturated fatty acid is susceptible to nitration (41). However, we use saturated phospholipids that essentially do not induce such reactions (39, 40, 42). The mean particle diameter was regulated by an extrusion method to 265–305 nm to study the influence of $[Hb]_{in}$, and to 178, 265, and 452 nm at the same $[Hb]_{in}$ (equal to 35 g/dl) to study the influence of the particle diameter (32, 34, 43, 44) (Table 1). After removing the unencapsulated Hb solution using ultracentrifugation, HbV was resuspended in the same PBS solution (pH 7.4) at [heme] = 300 μM. Therefore, the carbonylhemoglobin in HbV is converted to $HbO_2$ by photodissociation of CO by illuminating visible light under $O_2$ atmosphere. Briefly, an aliquot of CO-bound HbV was put in a glass flask; this was rotated using a rotary evaporator while the flask was immersed in cold water and illuminated using a halogen lamp (500 watts) with a continuous and gentle $O_2$ flow inside the flask for several minutes. The complete conversion to $HbO_2$ was confirmed by absorption spectroscopy in the *Q* band. The physicochemical characteristics of the obtained HbVs are listed in Table 1. The particle size distribution was measured using a dynamic light-scattering method (Submicron Particle Size Analyzer, model N4 PLUS; Beckman-Coulter, Inc., Fullerton, CA). The $P_{50}$ values were obtained from the oxygen equilibrium curve measured with a Hemox-Analyzer (TCS Medical Science, Philadelphia, PA); all samples were ~13–16 torrs at 37 °C.

*Stopped-flow Analyses*—The time course of the ligand binding was analyzed at a rapid mixing of a deoxygenated HbV solution and a NO-containing or CO-containing solution using a stopped-flow rapid scan spectrophotometer (model RSP-1000; Unisoku Co. Ltd., Osaka, Japan). Solutions in the two reservoirs (A and B) are mixed rapidly with an applied pressure of 0.3–0.6 megapascals and a dead time for mixing of <1.5 ms. All measurements were performed at 25 °C. A PBS solution (3 ml each) was poured into both reservoirs and sealed using septum rubber seals. The reservoirs were deoxygenated by $N_2$ bubbling for over 30 min for the complete removal of $O_2$. This is important in the case of NO bubbling to prevent the NO loss and metHb formation. The HbV stock solution (~30 μl, [heme] = 300 μM) was injected into Reservoir A to adjust [heme] finally to 3 μM; the $N_2$ bubbling was changed to flowing to avoid denaturation of the solutes. Complete deoxygenation was confirmed using preliminary stopped-flow measurements (wavelength: 385–593 nm), where the Soret band showed a maximum absorption ($\lambda_{max}$) at 430 nm attributable to the presence of deoxyHb. In Reservoir B, NO or CO gas bubbling was started; a gentle $N_2$ flowing was maintained in Reservoir A. The mixed gases for NO binding (NO, 0.2029%; $N_2$, 99.7971%) and for CO binding (CO, 14.14%; $N_2$, 85.86%) were purchased from Takachiho Chemical Industrial Co., Ltd. (Tokyo). After about 10 min of bubbling, stopped flow measurement was initiated. The sampling interval and the exposure time were set as 1 ms. The measurement time was 210 ms. All measurements were performed three times, and the change of absorbance at 430 nm was plotted as a function of time. The apparent binding rate constants of NO and CO ($k'_{on}{}^{(NO)}$, and $k'_{on}{}^{(CO)}$, respectively) were calculated using Equation 1 under the assumption of homogeneous distribution

of Hb, irreversible second order reaction, and pseudo-first-order reaction when gas molecules are abundant,

$$\ln\frac{\Delta A_t}{\Delta A_0} = -k'_{on} \cdot C_{Gas} \cdot t \qquad \text{(Eq. 1)}$$

where $\Delta A_t$ represents the change of absorbance at 430 nm at time $t$ (equal to $A_t - A_{t=\infty}$), and $\Delta A_0$ is the absorbance at the initial time (equal to $A_{t=0} - A_{t=\infty}$). $C_{Gas}$ is the initial gas concentration. In the case of the NO binding experiment, NO (1.9 $\mu$M) is not excessively abundant in comparison with heme concentration (1.5 $\mu$M); therefore, we calculated the apparent binding rates from the slopes of the initial phase of reactions.

*Computer Simulation*—We assumed that HbV is spherical and dispersed homogeneously. The gas diffusion constants are much larger than those of Hb molecule (7 nm) and HbV (250 nm) (45). Accordingly, we analyzed only gas diffusion and the formation of ligand-bound Hb in a single HbV particle. We did not consider the extracellular diffusion barrier because of the rapid mixing of small particles, and also we did not consider the gas permeability constant in the lipid bilayer, because the thickness of the lipid bilayer (~5 nm) is thin in comparison with the particle diameter. (Our results show that they would not be important parameters in our system.) To simplify the equation, the distance from the surface to the core of HbV, 125 nm, was divided by 12.5 nm into 10 units. For simulation of a larger particle, such as that with an 8000-nm diameter, 4000 nm was divided by 12.5 nm into 320 units. The first unit is located at the HbV surface and is in the concentration boundary condition. The last unit is located in the core of HbV in the closed condition. From the gas diffusion equation (Equation 2), the one-dimensional diffusion from the surface to the core of the particle can be expressed as Equation 3,

$$\frac{\partial C_{Gas}}{\partial t} = D\frac{\partial^2 C_{Gas}}{\partial x^2} \qquad \text{(Eq. 2)}$$

$$\Delta C_{Gas}(t_i, x_j) = D \cdot \left(\frac{-A_j \cdot (C_{Gas}(t_i, x_j) - C_{Gas}(t_i, x_{j-1})) + A_{j+1} \cdot (C_{Gas}(t_i, x_{j+1}) - C_{Gas}(t_i, x_j))}{V_j \cdot \Delta x}\right) \cdot \Delta t \qquad \text{(Eq. 3)}$$

where $C_{Gas}(t_i, x_j)$ represents the gas concentration at time $i$ ($t_i$) in 1 unit ($x_j$; distance from the surface of HbV); $\Delta C_{Gas}(t_i, x_j)$ is a mass change by diffusion; $A_j$ is the interface area of the units $j-1$ and $j$, and it changes with the distance from the core of HbV; $\Delta t$ is the step time; $V_j$ is the volume of the unit $j$; and $\Delta x$ is the distance between neighboring units. A gas molecule reacts with a heme in Hb. We assumed that the reaction is irreversible. Therefore, the changes of concentrations are expressed as Equations 4 and 5 with a binding rate constant, $k_{on}$, of an elementary gas binding reaction.

$$\frac{dC_{heme}}{dt} = -k_{on} \cdot C_{Gas} \cdot C_{heme} \qquad \text{(Eq. 4)}$$

$$\frac{dC_{Gas}}{dt} = \frac{dC_{heme}}{dt} \qquad \text{(Eq. 5)}$$

At a step time $\Delta t$ and in a step unit $\Delta x$, the changes of concentrations ($\Delta C_{heme}$, $\Delta C'_{Gas}$) by the gas bindings are expressed as Equations 6 and 7.

$$\Delta C_{heme}(t_i, x_j) = -k_{on} \cdot C_{Gas}(t_i, x_j) \cdot C_{heme}(t_i, x_j) \cdot \Delta t \qquad \text{(Eq. 6)}$$

$$\Delta C'_{Gas}(t_i, x_j) = -k_{on} \cdot C_{Gas}(t_i, x_j) \cdot C_{heme}(t_i, x_j) \cdot \Delta t \qquad \text{(Eq. 7)}$$

**TABLE 2**
**Parameters for computer simulations for each HbV with different $[Hb]_{in}$**

| Parameters | Values | | | |
|---|---|---|---|---|
| Diameter (nm) | 50, 100, 200, 250, 500, 1000, 2000, 8000 | | | |
| [heme] in solution ($\mu$M) | 1.5 | | | |
| Initial [NO] in solution ($\mu$M) | 1.9 | | | |
| Initial [CO] in solution ($\mu$M) | 67.5 | | | |
| $k_{on}^{(NO)}$ ($M^{-1}$ $s^{-1}$) | $2.7 \times 10^7$ | | | |
| $k_{on}^{(CO)}$ ($M^{-1}$ $s^{-1}$) | $3.4 \times 10^7$ | | | |
| | 1 g/dl $[Hb]_{in}$ | 10 g/dl $[Hb]_{in}$ | 20 g/dl $[Hb]_{in}$ | 35 g/dl $[Hb]_{in}$ |
| $[heme]_{in}$ ($\mu$M) | 620 | 6200 | 12400 | 21700 |
| $D_{Hb}$ in HbV ($\mu m^2$ $s^{-1}$) | 77 | 53 | 29 | 7.4 |
| $D_{NO}$ in HbV ($\mu m^2$ $s^{-1}$)[a] | 2080 | 1590 | 1160 | 706 |
| $D_{CO}$ in HbV ($\mu m^2$ $s^{-1}$)[a] | 2150 | 1640 | 1200 | 731 |

[a] $D_{NO}$ in saline is 2210 $\mu m^2$ $s^{-1}$ and $D_{CO}$ in saline is 2290 $\mu m^2$ $s^{-1}$. $D_{Hb}$ in HbV is much smaller than $D_{NO}$ and $D_{CO}$. For that reason, we did not use $D_{Hb}$ in computer simulations. Consequently, we did not consider the so-called "facilitated gas diffusion" attributable to the diffusion and dissociation of HbNO or HbCO because of the low $D_{Hb}$ and the significantly large equilibrium constants of HbNO and HbCO in comparison with that of $HbO_2$.

At the onset of reaction by mixing two solutions in the stopped-flow apparatus, the gas diffuses into the HbV. Therefore, the initial unbound free gas concentration inside the vesicle is assumed to be zero. The initial unbound free heme concentrations of HbV are 620–21,700 $\mu$M ($[Hb]_{in}$ = 1–35 g/dl); they decrease with the reactions of gas molecules. All initial values for calculations are summarized in Table 2. The diffusion constant of the Hb molecule is concentration-dependent and decreases from 77 to 7.4 $\mu m^2$ $s^{-1}$ with increasing $[Hb]_{in}$ from 1 to 35 g/dl (46–48). The diffusion constants of gases are 2 orders larger than that of Hb. The diffusion constant of $O_2$ in Hb solutions ($D_{O_2}$) decreases with increasing Hb concentration. The diffusion constants of CO and NO ($D_{NO}$ and $D_{CO}$, respectively) are calculated from $D_{O_2}$ using Equation 8 (2),

$$D_x = D_{O_2} \cdot \left(\frac{32}{MW_x}\right)^{1/2} \qquad \text{(Eq. 8)}$$

where $MW_x$ is the molecular weight of NO or CO.

One-dimensional diffusion simulation coupled with gas binding reactions was performed based on the equations given above (Equations 3, 6, and 7) according to the finite differential method using a Visual Basic Language Programming (Excel, Microsoft Corp., Japan, Tokyo) in a personal computer. Both $C_{Gas}$ and $C_{heme}$ at $t_i$ were calculated using those at $t_{i-1}$. Both $\Delta C_{heme}$ and $\Delta C'_{Gas}$ were calculated using Equations 6 and 7. Gas molecules diffuse depending on a concentration gradient, and the obtained $\Delta C_{Gas}$ of Equation 3 was combined with $\Delta C'_{Gas}$ of Equation 7 for the next step calculation of $C_{Gas}$. The time interval, $\Delta t$, was set as 0.01 $\mu$s, and $10^7$ steps were required to calculate the reaction profile for 100 ms in the case of HbV with a 250-nm diameter. The data were output at every 5 ms.

As the reaction proceeds, the concentration of gas in the bulk solution decreases. To reflect this, Equation 9 is used,

$$C_2(\text{Gas}) = \frac{C_0(\text{Gas}) - C_1(\text{GasTotal}) \cdot \left(\frac{C_0(\text{heme})}{C_1(\text{heme})}\right)}{\left(1 - \frac{C_0(\text{heme})}{C_1(\text{heme})}\right)} \quad \text{(Eq. 9)}$$

where the following variables are used. $C_0$(Gas) is the initial gas concentration; $C_2$(Gas) is at the boundary condition (in the bulk solution); $C_1$(GasTotal) is the sum of the bound and unbound gas molecules in HbV; $C_0$(heme) is the total heme concentration in the solution (1.5 $\mu$M); and $C_1$(heme) is the heme concentration in HbV (such as 21,700 $\mu$M at $[Hb]_{in}$ = 35 g/dl).

The level of unbound free heme, $R$, can be expressed as Equation 10, which is used to calculate the levels of reactions for 100 ms and the apparent rate constants from the initial slopes (5 ms).

$$R = \frac{\sum_j V_j \cdot C_{\text{heme}}(t_i, x_j)}{\sum_j V_j \cdot C_{\text{heme}}(t_0, x_j)} \quad \text{(Eq. 10)}$$

## RESULTS

*NO Binding and CO Binding Profiles of HbV Using Stopped-flow Spectrophotometry*—The complete deoxygenation of HbV was clearly confirmed according to the characteristic wavelength of the maximum absorption ($\lambda_{max}$) at 430 nm. Because of the strong light-scattering effect of the HbV suspension in comparison with Hb solution and RBC (49), the absorption peaks in the $Q$ band region were not clear in this measurement. After rapid mixing with NO, the immediate absorbance reduction at 430 nm and the increase at 418 nm that correspond to the formation of nitrosylhemoglobin were confirmed (Fig. 1). In the case of mixing with CO, the immediate absorption increase at 419 nm was confirmed. The change of absorption at 430 nm in both reactions was single exponential and indicative of the formation of nitrosylhemoglobin or carbonylhemoglobin in the vesicles.

*Time Courses of NO Binding and CO Binding to HbV with Various $[Hb]_{in}$*—The scans of spectrophotometry in Fig. 1 were performed three times, and the average level of reaction was plotted as a ratio of absorbance at 430 nm ($\Delta A_t$) at time $t$, to the initial absorbance ($\Delta A_0$) at time 0 (Fig. 2). The *graph* shows that the NO binding is retarded with increasing $[Hb]_{in}$ from 1 to 35 g/dl. However, no such change was observed in the case of CO binding. From the slopes shown in Fig. 2, the apparent binding rate constants of $k'_{on}{}^{(NO)}$ for NO and $k'_{on}{}^{(CO)}$ for CO were obtained according to Equation 1 and were plotted against $[Hb]_{in}$ (Fig. 3*A*). This clearly shows that $k'_{on}{}^{(NO)}$ is dependent on $[Hb]_{in}$; it decreases from $2.6 \times 10^7$ to $0.9 \times 10^7$ $M^{-1}$ $s^{-1}$ with increasing $[Hb]_{in}$ from 1 to 35 g/dl. It must be emphasized that $k'_{on}{}^{(NO)}$ at $[Hb]_{in}$ = 1 g/dl was almost identical to $k_{on}{}^{(NO)}$ of a cell-free Hb solution ($2.7 \times 10^7$ $M^{-1}$ $s^{-1}$). On the other hand, $k'_{on}{}^{(CO)}$ values at $[Hb]_{in}$ = 1 and 35 g/dl were $3.1 \times 10^5$ and $3.0 \times 10^5$ $M^{-1}$ $s^{-1}$, respectively, and almost identical at any $[Hb]_{in}$ and even to $k_{on}{}^{(CO)}$ of a cell-free Hb solution.

*Time Courses of NO Binding and CO Binding to HbV with Different Particle Sizes*—The influence of particle size was investigated. At the same $[Hb]_{in}$ (35 g/dl), HbVs with different particle sizes were prepared. As shown in Fig. 3*B*, $k'_{on}{}^{(NO)}$ decreased from $1.5 \times 10^7$ $M^{-1}$ $s^{-1}$ to $6.5 \times 10^6$ $M^{-1}$ $s^{-1}$ with increasing the diameter from 178 ± 74 to 452 ± 184 nm. On the other hand, CO binding showed no such remarkable changes.

*Computer Simulations of NO Binding and CO Binding to HbV*—Computer simulations of the experimental results of NO and CO bindings to HbV at different $[Hb]_{in}$ (1–35 g/dl) and different particle diameters (50, 100, 200, 250, and 500 nm) were performed, and the obtained $k'_{on}{}^{(NO)}$ and $k'_{on}{}^{(CO)}$ were plotted on Fig. 3. It was clearly recreated that the NO binding is influenced significantly by $[Hb]_{in}$ and the particle size. Although there were deviations from the experimental results, the NO binding was retarded with increasing $[Hb]_{in}$ from 1 to 35 g/dl. On the other hand, no such change existed in the case of CO binding, and the simulations fit well with the experimental results (Fig. 3*A*). The

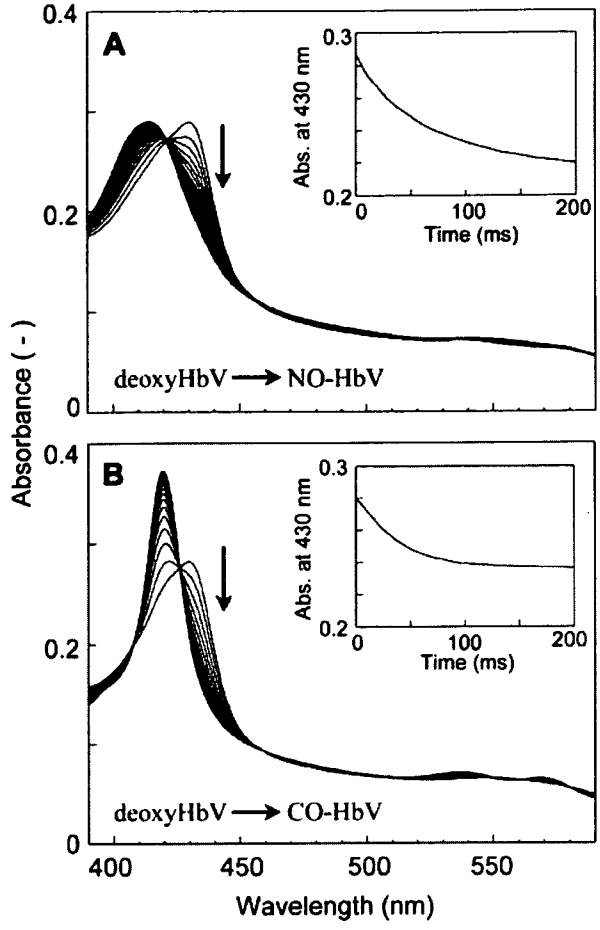


FIGURE 1. **Representative profiles of the reactions of NO or CO with deoxygenated HbV ($[Hb]_{in}$ = 35 g/dl) using stopped-flow spectrophotometry.** *A*, a NO-bubbled PBS ([NO] = 3.8 $\mu$M) and HbV in PBS ([heme] = 3.0 $\mu$M) were mixed rapidly using a stopped-flow spectrophotometer; the absorption spectra were collected every millisecond over 0.2 s after mixing. In this figure, the spectroscopic curves of every 10 ms are selected. This *panel* shows clearly that the spectrum of deoxyHbV is mostly converted to NO-HbV in 0.2 s. *Inset*, the time course of the measured absorbance at 430 nm. *B*, a CO-bubbled PBS ([CO] = 135 $\mu$M) and HbV in PBS ([heme] = 3.0 $\mu$M) were mixed rapidly using a stopped-flow spectrophotometer; the absorption spectra were collected every millisecond over 0.2 s after mixing. In this *panel*, the spectroscopic curves of every 10 ms were selected. This *panel* clearly shows that the spectrum of deoxyHbV is mostly converted to CO-HbV in 0.2 s. *Inset*, the time course of the measured absorbance at 430 nm. The optical path length was 1 cm. All of the experiments were performed at 25 °C.

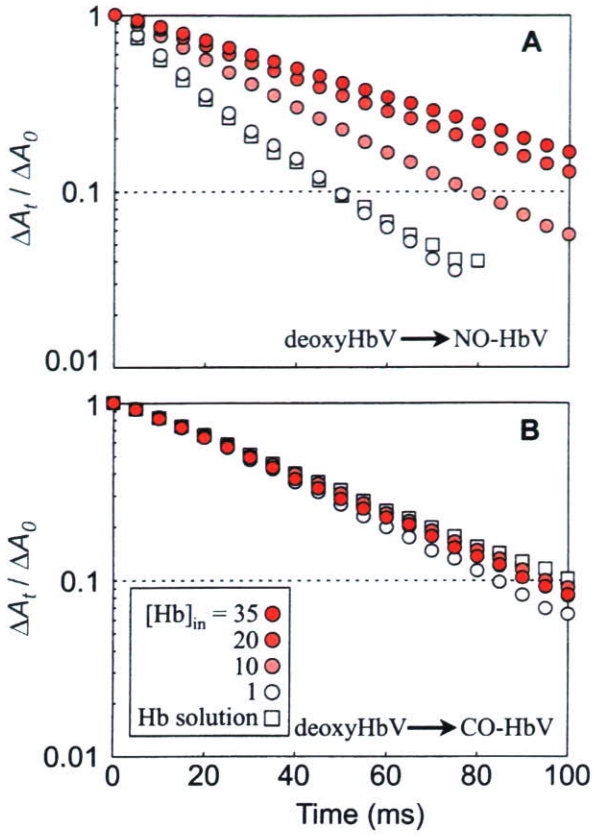


FIGURE 2. **Time courses of NO binding and CO binding by deoxygenated HbV with various [Hb]$_{in}$.** A NO-bubbled PBS (3.8 μM) (*A*) or a CO-bubbled PBS (135 μM) (*B*) and HbVs in PBS ([heme] = 3.0 μM) were mixed rapidly using a stopped-flow spectrophotometer. [Hb]$_{in}$ varies from 1 to 35 g/dl ([heme] = 620–21700 μM); thus, the number of particles differs at the constant [heme] (3.0 μM) in each solution. The level of reaction was plotted on a semilogarithmic *graph* as a ratio of absorption at 430 nm ($\Delta A_t$) at time *t*, to the initial absorption ($\Delta A_0$) at time 0. The results of the cell-free Hb solutions are also plotted, which are almost identical with those of HbV at [Hb]$_{in}$ = 1 g/dl. The *graph* shows that the NO binding rate is retarded with increasing [Hb]$_{in}$ in *A*. However, such a change was not apparent in the case of CO binding in *B*. All of the experiments were performed at 25 °C.

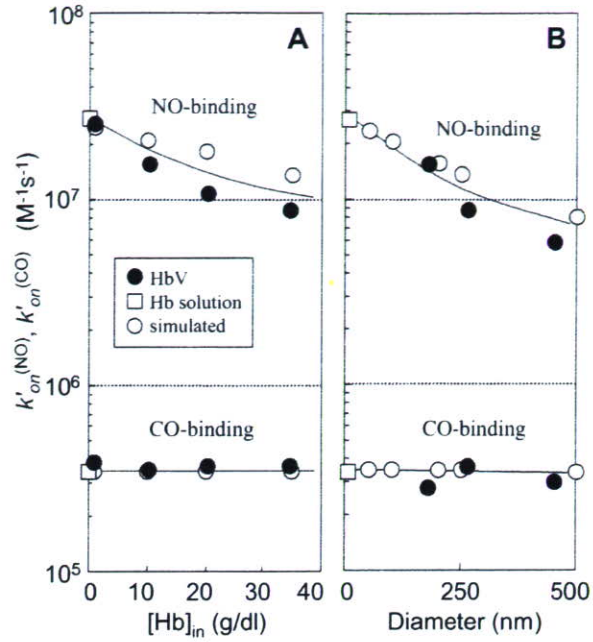


FIGURE 3. **Apparent binding rate constants of NO ($k'_{on}{}^{(NO)}$) and CO ($k'_{on}{}^{(CO)}$) of experimental results and computer simulations.** *A*, plotted against [Hb]$_{in}$ of HbV; *B*, plotted against particle diameter. *A*, the apparent binding rate constants (experimental) were calculated from the slopes in Fig. 2. Values of the exact $k_{on}{}^{(NO)}$ and $k_{on}{}^{(CO)}$ of the elementary reactions of cell-free Hb solution are also plotted on the *vertical axis*. Those of computer simulations (diameter, 250 nm) are plotted as *open circles*. *B*, the apparent binding rate constants were calculated similarly and plotted against the particle diameter. Values of the exact $k_{on}{}^{(NO)}$ and $k_{on}{}^{(CO)}$ of cell-free Hb solution (diameter, 7 nm) were also plotted. Those of computer simulations (diameter, 50, 100, 200, 250, and 500 nm) at [Hb]$_{in}$ = 35 g/dl are plotted as *open circles*. Both *graphs* show that computer simulations recreate well the tendencies of the experimental results; $k'_{on}{}^{(NO)}$ decreases considerably with increasing [Hb]$_{in}$ and diameter, and $k'_{on}{}^{(CO)}$ does not show such changes.

size dependence of $k'_{on}{}^{(NO)}$ and the independence of $k'_{on}{}^{(CO)}$ were also recreated well as shown in Fig. 3*B*. The larger particle showed a slower rate of NO binding but not CO binding. It should be noted that this simulation does not consider the extracellular diffusion barrier and lipid membrane permeability.

The one-dimensional concentration changes of free NO molecules and unbound free hemes in each unit in one HbV ([Hb]$_{in}$ = 1 and 35 g/dl) are obtained by simulations, and the results are converted to a two-dimensional scheme, as shown in Fig. 4. In the case of HbV at [Hb]$_{in}$ = 1 g/dl, both dissolved free NO and unbound free hemes are already homogeneously distributed at 5 ms, indicating that NO diffuses rapidly into HbV, and the reaction proceeds quite homogeneously. On the other hand, HbV at [Hb]$_{in}$ = 35 g/dl showed heterogeneous distribution. The concentration gradients of both NO and heme change from the interior surface to the core. Even after 100 ms, the distributions are heterogeneous.

To clarify the influence of $D_{NO}$ that changes with [Hb]$_{in}$ (Table 2), $D_{NO}$ was fixed to the value in the bulk solution (2210 $\mu m^2\ s^{-1}$) to all HbV with different [Hb]$_{in}$. As shown in Fig. 5, the difference in $k'_{on}{}^{(NO)}$ is minimized considerably in comparison with the condition of variable $D_{NO}$ at each [Hb]$_{in}$. This indicates that the lowered $D_{NO}$ in the highly concentrated viscous Hb solution contributes considerably to the retardation of NO binding.

*Extrapolation to Larger Particles (1000–8000 nm)*—Computer simulations were performed to larger particles (diameter, 1000, 2000, and 8000 nm) in addition to smaller particles (≤500 nm); their apparent binding rate constants, $k'_{on}{}^{(NO)}$ and $k'_{on}{}^{(CO)}$, are plotted against the diameter to clarify the influence of diameters of particles encapsulating the 1 and 35 g/dl Hb solutions (Fig. 6). The experimental values of the Hb solution and HbV are also plotted; they show good coincidence. At [Hb]$_{in}$ = 35 g/dl, both NO binding and CO binding are remarkably retarded with larger diameters. Interestingly, there were threshold diameters for retardation of both NO and CO bindings, around 100 nm for $k'_{on}{}^{(NO)}$ and 1000 nm for $k'_{on}{}^{(CO)}$. Although HbV with smaller diameters shows almost identical $k'_{on}{}^{(CO)}$, the results of our computer simulation suggest that particles larger than 1000 nm would show retardation of CO binding in much the same manner as that with NO binding. At [Hb]$_{in}$ = 1 g/dl, both NO binding and CO binding showed less change in the binding rate constants that coincide the experimental results; however, the simulation predicts that the retardation becomes obvious with particles larger than ~1000 nm for NO binding, and

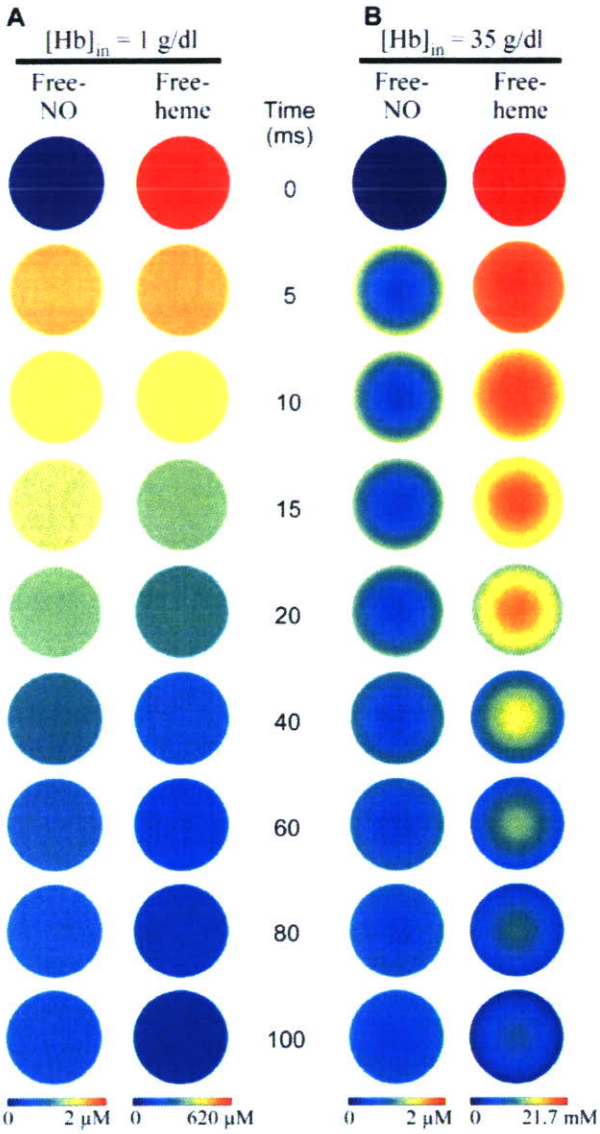


FIGURE 4. **Schematic two-dimensional representation of the simulated time courses of distributions of unbound free NO and unbound free heme in one HbV (250 nm).** *A*, at $[Hb]_{in}$ = 1 g/dl, both free NO and unbound hemes are distributed homogeneously at 5 ms, indicating that NO diffuses rapidly into HbV; the reaction proceeds homogeneously. *B*, at $[Hb]_{in}$ = 35 g/dl, both free NO and unbound hemes are distributed heterogeneously at any time. The concentration changes gradually from the surface to the core, indicating formation of the intracellular diffusion barrier. Particle diameter is fixed at 250 nm. It is easily speculated from the results that such gradients will be enhanced in larger particles.

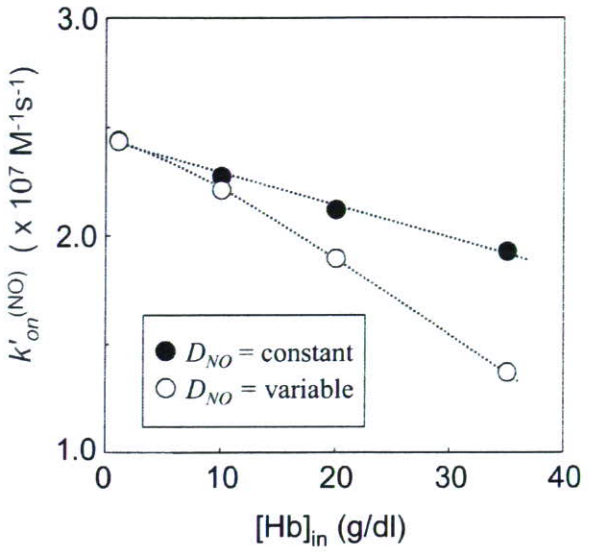


FIGURE 5. **Influence of $D_{NO}$ on the retardation of NO binding to HbV.** Computer simulations of NO binding to HbV were performed under the assumption that the diffusion constant of NO ($D_{NO}$) is independent of $[Hb]_{in}$ (*closed circles*). $D_{NO}$ was fixed to the value in the bulk solution (2210 $\mu m^2 s^{-1}$) to all HbV with different $[Hb]_{in}$. The HbV with a higher $[Hb]_{in}$ showed a slower rate of binding. However, the slope becomes gentle in comparison with the results of variable $D_{NO}$ at each $[Hb]_{in}$ as shown in Table 2 (*open circles*). This indicates the contribution of the reduced $D_{NO}$ in a highly viscous Hb solution to the retardation of NO binding. Particle diameter is fixed at 250 nm.

~2000 nm for CO binding. We can estimate the apparent binding rate constant of a particle encapsulating a 35-g/dl Hb solution with 8000-nm diameter, and $k'_{on}^{(NO)}$ and $k'_{on}^{(CO)}$ will be reduced to $5.6 \times 10^5$ and $7.3 \times 10^4$ $M^{-1}$ $s^{-1}$, respectively. Overall, encapsulation of a 35-g/dl Hb solution in an 8000-nm particle would retard the NO binding by 2 orders and the CO binding by 1 order in comparison with the corresponding elementary reactions of the cell-free Hb solution.

## DISCUSSION

Our primary finding is that NO binding of Hb is considerably retarded when a concentrated Hb solution is encapsulated in phospholipid vesicles (liposomes). On the other hand, CO binding of Hb shows no such retardation by encapsulation with particle size smaller than 500 nm. The phospholipid bilayer membrane itself has no barrier function to the gas diffusion, because the apparent binding rate constants of both NO and CO at $[Hb]_{in}$ = 1 g/dl and those of an acellular Hb solution were almost identical. In this study, using computer simulations, we propose that the determinant factor of retardation should be the intracellular, not extracellular, gas diffusion barrier in the case of HbV, which was induced by (i) the considerably large binding rate constant of NO to a heme of an Hb molecule, (ii) the numerous hemes as sites of gas entrapment at a high $[Hb]_{in}$, (iii) the slowed gas diffusion in the intracellular viscous Hb solution, and (iv) the longer diffusion distance in the larger particle diameter of the capsule (Fig. 7).

We reported the retardation of NO binding by Hb encapsulation in 1996 (30), which was earlier than the 1998 report of Liu *et al.* (6), who first showed that NO binding of Hb is retarded by the RBC cellular membrane. Rudolph *et al.* (26) attempted stopped-flow spectrophotometry of liposome-encapsulated Hb in 1997, expecting the retardation of the NO reaction by Hb encapsulation, but they identified no effect that was likely to have been attributable to the low $[Hb]_{in}$ (<14 g/dl) of their liposome-encapsulated Hb. In the present study, we intended more detailed analyses to clarify the mechanism of retardation, because it seems to have remained controversial in the last decade (20). It seems to us that these controversies are attributable to the complex and fragile structure of RBC and chemically unstable NO, which make it difficult to analyze the NO binding of RBC without causing hemolysis (2, 50). So-called competition experiments have been conducted between free Hb and RBC at a high hematocrit that would be a physiologically more

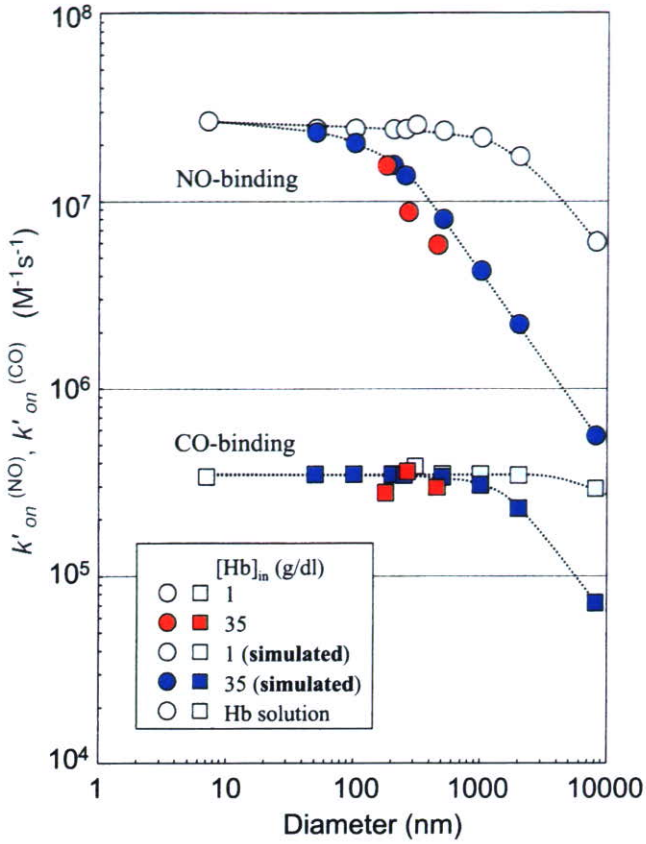


FIGURE 6. **Computer simulations of NO binding and CO binding by particles with different particle diameter.** At $[Hb]_{in}$ = 35 g/dl, the apparent CO binding rate constant, $k'_{on}{}^{(CO)}$, is almost identical up to 1000 nm in diameter; then it is reduced considerably, concomitant with increasing the diameter (*blue squares* in the *bottom*). On the other hand, $k'_{on}{}^{(NO)}$ decreases slightly up to 100 nm diameter; it then decreases steeply with enlarging particle diameter (*blue circles* in the *top*). In the case of $[Hb]_{in}$ = 1 g/dl, both NO binding (*light blue circles*) and CO binding (light blue squares) showed less change in the binding rate constants. However, the retardation becomes obvious when the particle diameter is larger than ~1000 nm for NO binding and even for CO binding when the diameter is larger than ~2000 nm. Experimental values for the Hb solution (*white circle* and *square*) and HbV (*pink* or *red squares* and *circles*) are close to the simulated values. The apparent binding rate constants, $k'_{on}{}^{(NO)}$ and $k'_{on}{}^{(CO)}$, of a spherical particle with diameter of 8000 nm and $[Hb]_{in}$ = 35 g/dl are estimated to be reduced to $5.6 \times 10^5$ and $7.3 \times 10^4$ $M^{-1}$ $s^{-1}$, respectively. The reported $k'_{on}{}^{(NO)}$ values of a series of chemically modified HBOCs (diameter, 6–28 nm), about $3.0 \times 10^7$ $M^{-1}$ $s^{-1}$, were identical to that of an unmodified Hb solution (38), which coincided well with our simulation.

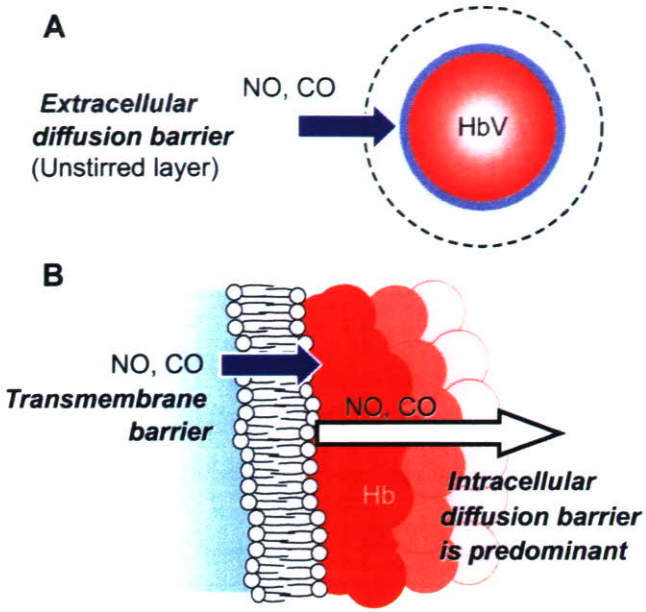


FIGURE 7. **Proposed mechanisms of retardation of gas binding by encapsulated Hbs.** *A*, it has been suggested that an unstirred layer near the outer surface of a cell would become an extracellular diffusion barrier to retard ligand bindings. However, our experimental results and computer simulations suggest that this is not a major process for retardation of ligand bindings in the case of HbV. *B*, the phospholipid bilayer membrane cannot have any barrier function to gas diffusion, because the apparent binding rate constants of both NO and CO at $[Hb]_{in}$ = 1 g/dl were close to those of an acellular Hb solution, as shown in Fig. 3. We propose that the determinant factor of retardation should be the intracellular diffusion barrier in the case of HbV, which is induced by (i) an intrinsically larger binding rate constant of NO to a heme in an Hb molecule, (ii) numerous hemes as sites of gas entrapment at a higher $[Hb]_{in}$, (iii) a slowed gas diffusion in the intracellular viscous Hb solution, and (iv) a longer gas diffusion distance in a larger capsule.

relevant condition (7, 50). However, it remains unclear for us whether the heterogeneous condition of a concentrated RBC suspension in a more static condition would be appropriate for an accurate kinetic measurement. Resealed RBCs were prepared to reduce the submembrane cytoskeletal layer or to reduce $[Hb]_{in}$ (2, 23), but it remains unknown whether hemolysis was suppressed completely after the complicated procedure and whether the electrolyte concentrations were maintained that might influence the Hb allostery and the resulting ligand binding profiles. We surmised that utilization of HbV, an artificially prepared model of RBC, would enable a systematic analysis, because the physicochemical parameters of HbV are adjustable, such as high $[Hb]_{in}$ up to 35 g/dl and particle diameter in a narrow range of $P_{50}$. Moreover, the physical stability of HbV is unexpectedly sufficient for stopped-flow spectrophotometry. We intentionally selected a low NO concentration (1.9 $\mu$M) to monitor the whole reaction of NO binding. Precedent reports of stopped-flow spectrophotometry of RBC at a higher NO concentration presented the problem not only of hemolysis but also the rate of NO reaction. It is so fast that a substantial part of the process occurs during the dead time (1–2 ms). On the other hand, in our study, a pseudo-first-order reaction is not appropriate for NO binding, and we calculated $k'_{on}{}^{(NO)}$ from the initial phase of the reaction because of a low NO concentration compared with the heme concentration. In such a condition, some redox charge transfer reaction would occur between heme and NO at a lower NO concentration (51). Another limitation of our simulation is the wide size distribution of HbV prepared using the extrusion method. $[Hb]_{in}$ was the concentration of the fed Hb solution for encapsulation, and we did not directly measure $[Hb]_{in}$ after encapsulation. These would be reasons for the deviation of the experimental results and the simplified computer simulation. However, it should be noted that our computer simulations recreated the tendencies of the experimental results of the ligand binding profiles of HbV.

In the computer simulation, we did not include the extracellular diffusion barrier, because HbV (250 nm) is much smaller than RBC (8 $\mu$m), and the diffusion of HbV as a particle should be much faster than that of RBC according to the Stokes-Einstein equation. The extracellular fluid near the surface should be stirred by the rapid movement of HbV. It is expected that the

thickness of the unstirred layer as an extracellular diffusion barrier would be much less for small HbV than that for RBC (1–3 μm) (2). Actually, results of the present computer simulations of HbV without consideration of the extracellular diffusion barrier clarified that the intracellular diffusion resistance is sufficient to explain the retardation of NO binding in the results of stopped-flow spectrophotometry, and possibly, our findings might suggest that the extracellular diffusion barrier is negligible even for RBC. This supports the results of Vaughn *et al.* (7) that the extracellular diffusion resistance is negligible. However, our data do not directly support the presence of transmembrane diffusion limitation, because the HbV at $[Hb]_{in}$ = 1 g/dl and the cell-free Hb solution showed nearly identical $k'_{on}{}^{(NO)}$; actually, the computer simulation did not require the consideration of the membrane barrier. Han *et al.* (23) proposed that a submembrane cytoskeletal barrier would induce the resistance to the NO binding to bovine RBC using the RBC ghost. This might be possible to some extent if the submembrane cytoskeleton were to contain densely layered heme proteins such as adsorbed Hbs that could be the sites of rapidly binding NO. However, we believe that the intracellular concentrated Hb solution (about 35 g/dl) near the cytoskeleton of RBC can be the predominant barrier to further NO diffusion into RBC. Liu *et al.* (19) described that "NO that enters into RBC is immediately scavenged by the concentrated intracellular Hb so that NO concentration inside the RBC is maintained very close to zero," although they did not pay attention to it as the intracellular diffusion barrier.

The binding rate constant of CO of cell-free Hb molecule ($k_{on}{}^{(CO)}$) is well known to be much smaller than those of NO and $O_2$ (52). The rate-limiting step for CO binding is the internal bond formation with the heme iron. In fact, based on the electron theory, CO enters the globin hundreds of times before it finally forms a bond with the iron atom. Consequently, the overall bimolecular rate constant is normally small (53). The experimental finding that CO binding shows negligible retardation, even after encapsulation in HbV, also supports our proposal that rapid NO binding causes the sink of NO at the interior surface region of HbV and retards further NO diffusion into the core of HbV in combination of the lowered $D_{NO}$ in the highly concentrated viscous Hb solution (45–48). However, it is expected that HbV with a much larger diameter can contribute to retardation, even for CO binding, as clarified by our computer simulation. Coin and Olson (2) compared the bindings of $O_2$, CO, and ethyl isocyanate to Hb with their elementary reaction constants, $k_{on}$, of $3 \times 10^6$, $2.0 \times 10^5$, and $2.1 \times 10^4$ $M^{-1}$ $s^{-1}$, respectively (1:10 and 1:100 differences). Results of that study showed that the difference between $k_{on}$ of Hb and $k'_{on}$ of RBC decreases for a slower reaction. The difference becomes very small for the binding of ethyl isocyanate, which clearly supports our data; a faster reaction tends to induce a stronger intracellular diffusion barrier and retards the reaction in comparison with the cell-free Hb solution.

In blood circulation in the presence of $O_2$, NO is inactivated mainly by NO dioxygenation by $O_2$-bound HBOCs and RBC. According to Herold *et al.* (54), the rate constant of the elementary reaction, $HbO_2$ and NO, is $8.9 \times 10^7$ $M^{-1}$ $s^{-1}$, which is faster than that of deoxyHb ($2.6 \times 10^7$ $M^{-1}$ $s^{-1}$). We predict that the reaction with $HbO_2$ should be much faster to form an intracellular diffusion barrier than that with deoxyHb. Consequently, the contribution of Hb encapsulation to the retardation should be pronounced. This can support the results of Azarov *et al.* (50) and Huang *et al.* (21), which showed that "the membrane barrier function" becomes more effective in limiting NO uptake for oxygenated RBC than the deoxygenated RBC, although their proposing mechanism is different from ours.

Our computer simulation system would be an effective tool to predict the ligand binding profiles of HbV with different Hb concentration and different particle size and other imaginary parameters. This can roughly simulate the NO binding and CO binding profiles of a spherical particle with a diameter identical to that of the major axis of RBC. The values of $k'_{on}{}^{(NO)}$ and $k'_{on}{}^{(CO)}$ of a spherical particle encapsulating 35-g/dl Hb with a diameter of about 8 μm are estimated, respectively, as $5.6 \times 10^5$ and $7.3 \times 10^4$ $M^{-1}$ $s^{-1}$. Those values resemble the precedent values of human RBC measured using stopped-flow spectrophotometry without causing hemolysis (<5%): $k'_{on}{}^{(NO)}$, $1.2 \times 10^5$ $M^{-1}$ $s^{-1}$; $k'_{on}{}^{(CO)}$, $6.5 \times 10^4$ $M^{-1}$ $s^{-1}$ (55); and $k'_{on}{}^{(CO)}$, $6.0 \times 10^4$ $M^{-1}$ $s^{-1}$ (31). On the other hand, our simulated $k'_{on}{}^{(NO)}$ would be faster than the values of RBC; $5.2 \times 10^4$ $M^{-1}$ $s^{-1}$ (6) and $1.4 \times 10^4$ $M^{-1}$ $s^{-1}$ (50), which are contradictorily much smaller than the CO binding rate constants of the above, which might suggest the presence of other mechanisms, such as the unstirred layer as the extracellular diffusion barrier in the case of large RBCs that diffuse slowly at a high Hct in their experiments. Even so, the retardation seems to be mainly induced by the intracellular diffusion barrier, because $k'_{on}{}^{(NO)}$ is reduced by 2 orders of magnitude in comparison with a cell-free Hb. Alternatively, we might consider the biconcave disk structure of RBC. Different $P_{50}$ values of HbV (13–16 torrs) in comparison with that of human RBC (28 torrs) might also influence the binding rates.

Interestingly, the presence of the threshold diameters for retardation of ligand bindings is apparent, as shown in Fig. 6. The threshold diameter for CO is larger than that for NO, indicating that the slower reaction of CO binding allows a longer distance of gas diffusion before induction of an intracellular diffusion barrier than it allows with the more rapid NO binding. The rate-determining steps are the elementary gas-binding reaction for particles smaller than the threshold diameter and the gas diffusion for larger particles. It should be noted that the retardation is predicted for the larger particles at $[Hb]_{in}$ = 1 g/dl, although the threshold diameter is increased to 1000 nm for NO binding and 2000 nm for CO binding.

The retardation of NO binding by Hb encapsulation cannot fully explain the phenomenon that HbV with a diameter of ~250 nm does not induce vasoconstriction after intravenous injection (13), because $k'_{on}{}^{(NO)}$ of HbV is much larger than that of RBC ($10^4$ to $10^5$ $M^{-1}$ $s^{-1}$). Any HBOC is much smaller in size than RBC and is distributed homogeneously in the plasma layer (5). Therefore, an RBC-free zone at the blood/endothelium interface becomes an HBOC-dissolved zone and might be a sink of NO (56, 57). Rohlfs *et al.* (38) reported that the NO binding rate constants of a series of chemically modified HBOCs (diameter, 6–28 nm) (58), measured using the laser flash photolysis, were identical to that of an unmodified Hb

solution, about $3.0 \times 10^7$ $M^{-1}$ $s^{-1}$, which coincided well with our simulation in Fig. 6; particles with a diameter of less than 50 nm are almost identical. They concluded straightforwardly that NO uptake was not related to vasoconstriction, because polyethylene glycol-modified Hb did not exceptionally induce vasoconstriction, and other mechanisms are actually suggested in relation to molecular recognition and oxygen affinity (11, 59). We speculate the presence of another threshold particle diameter to penetrate across the perforated endothelial cell layer to approach a space (such as the space of Disse near the sinusoidal endothelial layer in a hepatic microcirculation or the space between the endothelium and the smooth muscle) where CO or NO is produced as a vasorelaxation factor to bind to soluble guanylate cyclase, which catalyzes the conversion of guanosine triphosphate to cyclic guanosine monophosphate (13, 18, 60, 61). As summarized by Olson *et al.* (16), both the retardation of the NO reaction (reduced NO affinity) (62) and the larger particle diameter are inferred to be keys to suppress vasoconstriction and hypertension induced by HBOCs.

In summary, we suggest the significant contribution of the intracellular diffusion barrier and the absence of lipid membrane barrier for NO uptake in the case of HbV. We speculate that the same findings might apply to RBCs. Although some discrepancies exist between the experimental results and computer simulations, we are surprised that such a simple simulation system can be an effective tool to predict the ligand binding reaction of HbV and larger particles, although the system is based merely on physicochemical parameters: the gas diffusion constant and elementary reaction rate constants. Our data provide a new insight into the cellular structures of RBC and HbV as an artificial oxygen carrier. Our next step will be to apply this system to recreate the ligand binding profiles of a biconcave disk shaped or parachute-like RBC and HbV suspension flowing heterogeneously in microvessels and in an artificial gas-permeable narrow tube (5) to identify additional mechanisms of the absence of vasoconstriction.

*Acknowledgments—We thank Prof. M. Intaglietta (University of California, San Diego) and Prof. M. Suematsu (Keio University) for discussion related to the mechanism of ligand binding.*

## REFERENCES


1. Hartridge, H., and Roughton, F. J. W. (1927) *J. Physiol.* **62,** 232–242
2. Coin, J. T., and Olson, J. S. (1979) *J. Biol. Chem.* **254,** 1178–1190
3. Vandegriff, K. D., and Olson, J. S. (1984) *J. Biol. Chem.* **259,** 12619–12627
4. Page, T. C., Light, W. R., McKay, C. B., and Hellums, J. D. (1998) *Microvasc. Res.* **55,** 54–66
5. Sakai, H., Suzuki, Y., Kinoshita, M., Takeoka, S., Maeda, N., and Tsuchdia, E. (2003) *Am. J. Physiol.* **285,** H2543–H2555
6. Liu, X., Miller, M. J., Joshi, M. S., Sadowska-Krowicka, H., Clark, D. A., and Lancaster, J. R., Jr. (1998) *J. Biol. Chem.* **273,** 18709–19713
7. Vaughn, M. W., Huang, K. T., Kuo, L., and Liao, J. C. (2000) *J. Biol. Chem.* **275,** 2342–2348
8. Minneci, P. C., Deans, K. J., Zhi, H., Yuen, P. S., Star, R. A., Banks, S. M., Schechter, A. N., Natanson, C., Gladwin, M. T., and Solomon, S. B. (2005) *J. Clin. Invest.* **115,** 3409–3417
9. Hess, J. R., MacDonald, V. W., and Brinkley, W. W. (1993) *J. Appl. Physiol.* **74,** 1769–1778
10. Sloan, E. P., Koenigsberg, M., Gens, D., Cipolle, M., Runge, J., Mallory, M. N., and Rodman, G., Jr. (1999) *J. Am. Med. Assoc.* **282,** 1857–1864
11. Gulati, A., Barve, A., and Sen, A. P. (1999) *J. Lab. Clin. Med.* **133,** 112–119
12. Rochon, G., Caron, A., Toussaint-Hacquard, M., Alayash, A. I., Gentils, M., Labrude, P., Stoltz, J. F., and Menu, P. (2004) *Hypertension* **43,** 1110–1115
13. Sakai, H., Hara, H., Yuasa, M., Tsai, A. G., Takeoka, S., Tsuchida, E., and Intaglietta, M. (2000) *Am. J. Physiol.* **279,** H908–H915
14. Nakai, K., Ohta, T., Sakuma, I., Akama, K., Kobayashi, Y., Tokuyama, S., Kitabatake, A., Nakazato, Y., Takahashi, T. A., and Sekiguchi, S. (1996) *J. Cardiovasc. Pharmacol.* **28,** 115–123
15. Bunn, H. F. (1995) *Transfus. Clin. Biol.* **2,** 433–439
16. Olson, J. S., Foley, E. W., Rogge, C., Tsai, A. L., Doyle, M. P., and Lemon, D. D. (2004) *Free Radic. Biol. Med.* **36,** 685–697
17. Suematsu, M., Goda, N., Sano, T., Kashiwagi, S., Egawa, T., Shinoda, Y., and Ishimura, Y. (1995) *J. Clin. Invest.* **96,** 2431–2437
18. Goda, N., Suzuki, K., Naito, M., Takeoka, S., Tsuchida, E., Ishimura, Y., Tamatani, T., and Suematsu, M. (1998) *J. Clin. Invest.* **101,** 604–612
19. Liu, X., Samouilov, A., Lancaster, J. R., Jr., and Zweier, J. L. (2002) *J. Biol. Chem.* **277,** 26194–26199
20. Kim-Shapiro, D. B., Schechter, A. N., and Gladwin, M. T. (2006) *Arterioscler. Thromb. Vasc. Biol.* **26,** 697–705
21. Huang, K. T., Huang, Z., and Kim-Shapiro, D. B. (2007) *Nitric Oxide* **16,** 209–216
22. Huang, K. T., Han, T. H., Hyduke, D. R., Vaughn, M. W., Van Herle, H., Hein, T. W., Zhang, C., Kuo, L., and Liao, J. C. (2001) *Proc. Natl. Acad. Sci. U. S. A.* **98,** 11771–11776
23. Han, T. H., Pelling, A., Jeon, T. J., Gimzewski, J. K., and Liao, J. C. (2005) *Biochim. Biophys. Acta* **1723,** 135–142
24. Sakai, H., Masada, Y., Horinouchi, H., Yamamoto, M., Ikeda, E., Takeoka, S., Kobayashi, K., and Tsuchida, E. (2004) *Crit. Care Med.* **32,** 539–545
25. Sakai, H., Horinouchi, H., Yamamoto, M., Ikeda, E., Takeoka, S., Takaori, M., Tsuchida, E., and Kobayashi, K. (2006) *Transfusion* **46,** 339–347
26. Rudolph, A. S., Sulpizio, A., Hieble, P., MacDonald, V., Chavez, M., and Feuerstein, G. (1997) *J. Appl. Physiol.* **82,** 1826–1835
27. Chang, T. M. (2006) *Artif. Cells Blood Substit. Biotechnol.* **34,** 551–566
28. Djordjevich, L., and Miller, I. F. (1982) *Exp. Hematol.* **8,** 584–592
29. Sakai, H., Tomiyama, K. I., Sou, K., Takeoka, S., and Tsuchida, E. (2000) *Bioconjugate Chem.* **11,** 425–432
30. Sakai, H., Hamada, K., Takeoka, S., Nishide, H., and Tsuchida, E. (1996) *Polymer Adv. Technol.* **7,** 639–644
31. Olson, J. S. (1981) *Methods Enzymol.* **76,** 631–651
32. Takeoka, S., Ohgushi, T., Terase, K., Ohmori, T., and Tsuchida, E. (1996) *Langmuir* **12,** 1755–1759
33. Sakai, H., Tsai, A. G., Rohlfs, R. J., Hara, H., Takeoka, S., Tsuchida, E., and Intaglietta, M. (1999) *Am. J. Physiol.* **276,** H553–H562
34. Takeoka, S., Terase, K., Yokohama, H., Sakai, H., Nishide, H., and Tsuchida, E. (1994) *J. Macromol. Sci. Pure Appl. Chem., Part A* **31,** 97–108
35. Wang, L., Morizawa, K., Tokuyama, S., Satoh, T., and Tsuchida, E. (1992) *Polymer Adv. Technol.* **4,** 8–11
36. Sakai, H., Takeoka, S., Yokohama, H., Seino, Y., Nishide, H., and Tsuchida, E. (1993) *Protein Expression Purif.* **4,** 563–569
37. Sakai, H., Masada, Y., Takeoka, S., and Tsuchida, E. (2002) *J. Biochem. (Tokyo)* **131,** 611–617
38. Rohlfs, R. J., Bruner, E., Chiu, A., Gonzales, A., Gonzales, M. L., Magde, D., Magde, M. D. Jr., Vandegriff, K. D., and Winslow, R. M. (1998) *J. Biol. Chem.* **273,** 12128–12134
39. Szebeni, J., Breuer, J. H., Szelenyi, J. G., Bathori, G., Lelkes, G., and Hollan, S. R. (1984) *Biochim. Biophys. Acta* **798,** 60–67
40. Szebeni, J., Di Iorio, E. E., Hauser, H., and Winterhalter, K. H. (1985) *Biochemistry* **24,** 2827–2832
41. Baker, P. R., Lin, Y., Schopfer, F. J., Woodcock, S. R., Groeger, A. L., Batthyany, C., Sweeney, S., Long, M. H., Iles, K. E., Baker, L. M., Branchaud, B. P., Chen, Y. E., and Freeman, B. A. (2005) *J. Biol. Chem.* **280,** 42464–42475
42. Yokohama, H., Seino, Y., Chung, J., Sakai, H., Takeoka, S., Nishide, H., and Tsuchida, E. (1994) *Artif. Organs Today* **4,** 107–116
43. Sou, K., Naito, Y., Endo, T., Takeoka, S., and Tsuchida, E. (2003) *Biotechnol. Prog.* **19,** 1547–1552
44. Sakai, H., Hamada, K., Takeoka, S., Nishide, H., and Tsuchida, E. (1996) *Biotechnol. Prog.* **12,** 119–125
45. Nishide, H., Chen, X., and Tsuchida, E. (1997) *Artif. Cells Blood Substit.*